

Dynamical Mean-Field Theory of Complex Systems on Sparse Directed Networks

Fernando L. Metz

Physics Institute, Federal University of Rio Grande do Sul, 91501-970 Porto Alegre, Brazil

(Dated: January 23, 2025)

Although real-world complex systems typically interact through sparse and heterogeneous networks, analytic solutions of their dynamics are limited to models with all-to-all interactions. Here, we solve the dynamics of a broad range of nonlinear models of complex systems on sparse directed networks with a random structure. By generalizing dynamical mean-field theory to sparse systems, we derive an exact equation for the path-probability describing the effective dynamics of a single degree of freedom. Our general solution applies to key models in the study of neural networks, ecosystems, epidemic spreading, and synchronization. Using the population dynamics algorithm, we solve the path-probability equation to determine the phase diagram of a seminal neural network model in the sparse regime, showing that this model undergoes a transition from a fixed-point phase to chaos as a function of the network topology.

Introduction. Complex dynamical systems are modeled by N degrees of freedom $x_i(t)$ ($i = 1, \dots, N$) that evolve in time according to the differential equation

$$\dot{x}_i(t) = -f(x_i) + \sum_{j=1}^N A_{ij}g(x_i, x_j), \quad (1)$$

where $\{A_{ij}\}_{i,j=1,\dots,N}$ defines the interaction network. The function $f(x)$ governs the dynamics in the absence of interactions, and the kernel $g(x, x')$ shapes the pairwise couplings. Equation (1) models the nonequilibrium dynamics of neural networks [1–5] and ecosystems [6–8], epidemic spreading [9–12], synchronization phenomena [13–15], opinion dynamics [16, 17], and multivariate Ornstein-Uhlenbeck processes [18–20]. Table I specifies $f(x)$ and $g(x, x')$ for paradigmatic models of complex behavior.

Model	$f(x)$	$g(x, x')$
Ornstein-Uhlenbeck process [18]	x	x'
SIS model of epidemic spreading [9]	x	$(1-x)x'$
Lotka-Volterra (LV) model [7, 8]	$x(x-1)$	xx'
Neural network (NN) model [1, 4]	x	$\tanh(x')$
Kuramoto model [14]	0	$\sin(x' - x)$

TABLE I. Explicit form of $f(x)$ and $g(x, x')$ in complex systems modeled by Eq. (1). Equation (1) for the SIS model is derived through the quenched mean-field approximation [12, 21, 22].

The foremost problem in the study of complex systems is how to reduce the dynamics of many interacting elements to the dynamics of a few variables [23]. Dynamical mean-field theory (DMFT) [24–26] is a powerful method to tackle this problem in the limit $N \rightarrow \infty$, yielding a solution in terms of the path-probability for the effective dynamics of a single degree of freedom. The application of DMFT to models described by Eq. (1) has been attracting an enormous interest [2–5, 7, 8, 15, 19, 20, 27–34], especially in the context of neural networks and ecosystems. Phase diagrams of these models reveal a rich

phenomenology, including different types of phase transitions [5, 7, 30], chaotic behavior [1, 3], and coexistence of multiple attractors [7, 8, 35]. Despite this substantial theoretical progress, DMFT is currently limited to dense networks, where each dynamical variable is essentially coupled to *all* others by means of Gaussian interaction strengths. However, the interactions in real-world complex systems are known to be *sparse* and *heterogeneous* [36, 37]. Sparseness indicates that each element of the system interacts on average with a finite number of others, while heterogeneity refers to fluctuations in the local topology of the interaction network. How to integrate these more realistic features in the formalism of DMFT for systems modeled by Eq. (1) remains an unresolved challenge, and even basic questions, such as deriving the phase diagram of sparse complex systems, are still out of reach.

On the other hand, the dynamics of complex systems on sparse networks has been extensively studied in the case of Ising spins [38–50]. In this context, both the cavity method [39] and DMFT [38, 40] provide an analytic solution in terms of the path-probability for the effective dynamics of a single dynamical variable. However, the presence of bidirected edges induces a temporal feedback, which, in the particular case of sparse systems, leads to an exponential growth of the path-probability dimension [38, 40, 49], rendering numerical computations unfeasible. Approximation schemes, such as the one-time approximation [39], make these computations possible [42, 43, 48]. When the interactions are directed or unidirectional, there is no temporal feedback and the path-probability equation can be efficiently solved [38, 39, 51].

Inspired by these results for Ising spins, in this Letter we solve the dynamics of models governed by Eq. (1) on sparse directed networks with an heterogeneous topology. The solution represents a foundational step in the study of complex systems, as it ultimately incorporates the sparse and heterogeneous structure of complex networks into the formalism of DMFT. Directed networks are interesting because they model the non-reciprocal in-

interactions in real-world complex systems [52], including the human cortex [53], food-webs [37, 54, 55], gene regulatory networks [56, 57], online social networks [58, 59], and the World Wide Web [60]. The formalism presented here thus opens the possibility to analytically investigate how realistic interactions impact the dynamics of complex systems.

By generalizing DMFT to sparse systems, we obtain an exact equation for the path-probability describing the effective dynamics of a single variable for $N \rightarrow \infty$, and we solve this equation for different models in table I by using the population dynamics algorithm [61–66]. The excellent agreement between our theoretical results and numerical simulations of finite systems confirms that our solution applies to various nonlinear models interacting through different network topologies, including networks with power-law degree distributions [36].

As an application, we determine the phase diagram of the neural network model by Sompolinsky *et al* [1] in the sparse regime. We show that the phase diagram displays trivial and nontrivial fixed-point phases, a chaotic phase with zero mean activity, and a chaotic phase with nonzero mean activity [30]. By calculating certain macroscopic observables, we determine the transition lines as functions of the mean degree and the variance of the coupling strengths, showing their consistency with the universal critical lines derived from random matrix theory [67–69]. In particular, we provide numerical evidence that the transition between the chaotic phases coincides with the vanishing of the gap between the leading and the subleading eigenvalue of the interaction matrix.

Sparse directed networks. Let $A_{ij} = C_{ij}J_{ij}$ be the elements of the $N \times N$ interaction matrix \mathbf{A} . The binary variables $C_{ij} \in \{0, 1\}$ determine the network topology, while $J_{ij} \in \mathbb{R}$ controls the interaction strengths. If $C_{ij} = 1$, there is a directed edge $j \rightarrow i$ pointing from node j to i , while $C_{ij} = 0$ otherwise. The indegree $K_i = \sum_{j=1}^N C_{ij}$ and the outdegree $L_i = \sum_{j=1}^N C_{ji}$ count the number of links entering and leaving node i [36], respectively. The random variables $\{C_{ij}\}_{i \neq j}$ follow the distribution

$$\mathbb{P}(\{C_{ij}\}) = \frac{1}{\mathcal{N}} \prod_{i \neq j=1}^N \left[\frac{c}{N} \delta_{C_{ij},1} + \left(1 - \frac{c}{N}\right) \delta_{C_{ij},0} \right] \times \prod_{i=1}^N \delta_{K_i, \sum_{j=1}^N C_{ij}} \delta_{L_i, \sum_{j=1}^N C_{ji}}, \quad (2)$$

where \mathcal{N} is the normalization constant and $C_{ii} = 0$. The degrees $\{K_i, L_i\}_{i=1, \dots, N}$ are independent and identically distributed random variables drawn from $p_{k,\ell} = p_{\text{in},k} p_{\text{out},\ell}$, where $p_{\text{in},k}$ and $p_{\text{out},\ell}$ are the indegree and the outdegree distribution [36, 64], respectively. The parameter c is the average degree

$$c = \sum_{k=0}^{\infty} k p_{\text{in},k} = \sum_{\ell=0}^{\infty} \ell p_{\text{out},\ell}. \quad (3)$$

Equation (2) defines a network ensemble where directed links are randomly placed between pairs of nodes with probability c/N , subject to the prescribed degree sequences generated from $p_{k,\ell}$. In the limit $N \rightarrow \infty$, network samples generated from Eq. (2) are similar to those produced by the configuration model [70, 71]. The coupling strengths $\{J_{ij}\}_{i,j=1, \dots, N}$ are independent and identically distributed random variables drawn from a distribution p_J with mean μ_J and variance σ_J^2 . The distributions $p_{k,\ell}$ and p_J fully specify the network ensemble, allowing for a systematic investigation of how network heterogeneities impact the dynamics of complex systems.

Solution through DMFT. We solve the coupled dynamics of Eq. (1) on directed networks by using dynamical mean-field theory (DMFT) [24–26]. We consider the sparse regime, where the mean degree c is *finite*, independent of N . DMFT is based on the generating functional

$$\mathcal{Z}[\boldsymbol{\psi}] = \int \left(\prod_{i=1}^N Dx_i \right) \mathcal{P}[\mathbf{x}] e^{i \int dt \sum_{i=1}^N x_i(t) \psi_i(t)} \quad (4)$$

of the probability density $\mathcal{P}[\mathbf{x}]$ of observing a dynamical path of states $\mathbf{x}(t) = (x_1(t), \dots, x_N(t))$ in a fixed time interval. The correlation functions of $\{x_i(t)\}_{i=1, \dots, N}$ follow from the derivatives of $\mathcal{Z}[\boldsymbol{\psi}]$ with respect to the external sources $\boldsymbol{\psi}(t) = (\psi_1(t), \dots, \psi_N(t))$. The n th-moment of the local variable $x_i(t)$,

$$\langle x_i^n(t) \rangle = \int \left(\prod_{i=1}^N Dx_i \right) x_i^n(t) \mathcal{P}[\mathbf{x}] = (-i)^n \frac{\delta^n \mathcal{Z}[\boldsymbol{\psi}]}{\delta \psi_i^n(t)} \Big|_{\boldsymbol{\psi}=0}, \quad (5)$$

yields the time-evolution of the macroscopic quantities

$$m(t) = \lim_{N \rightarrow \infty} \frac{1}{N} \sum_{i=1}^N \langle x_i(t) \rangle, \quad q(t) = \lim_{N \rightarrow \infty} \frac{1}{N} \sum_{i=1}^N \langle x_i^2(t) \rangle. \quad (6)$$

Clearly, $\mathcal{Z}[\boldsymbol{\psi}]$ fulfills $\mathcal{Z}[0] = 1$.

In [72], we calculate the average of $\mathcal{Z}[\boldsymbol{\psi}]$ over the network ensemble defined by Eq. (2) for finite c , recasting the problem in terms of the solution of a saddle-point integral. More importantly, we give a clear physical interpretation of the order-parameters, simplifying the saddle-point equations and obtaining a feasible solution for the dynamics in the sparse regime. In the limit $N \rightarrow \infty$, the microscopic dynamical variables decouple, and the path-probability $\mathcal{P}[x]$ for the effective dynamics of a single variable $x(t)$ is determined from

$$\mathcal{P}[x] = \sum_{k=0}^{\infty} p_{\text{in},k} \int \left(\prod_{j=1}^k Dx_j \mathcal{P}[x_j] \right) \int \left(\prod_{j=1}^k dJ_j p_J(J_j) \right) \times \delta_F \left[\dot{x}(t) + f(x(t)) - \sum_{j=1}^k J_j g(x(t), x_j(t)) \right], \quad (7)$$

where δ_F is the functional Dirac- δ . The macroscopic observables are computed from $m(t) = \langle x(t) \rangle_*$ and $q(t) = \langle x^2(t) \rangle_*$, where

$$\langle x^n(t) \rangle_* = \int Dx x^n(t) \mathcal{P}[x] \quad (n = 1, 2) \quad (8)$$

is the average over the effective dynamics governed by $\mathcal{P}[x]$. The self-consistent Eq. (7) is the exact solution of a broad class of models (see table I) on sparse directed networks with a local treelike structure [73] and arbitrary distributions p_J and $p_{k,\ell} = p_{\text{in},k} p_{\text{out},\ell}$. In [72], we address the more general case of dynamical models with Gaussian additive noise on networks with correlated indegrees and outdegrees. The solution of Eq. (7) determines the time-evolution of the full probability distribution of the microscopic variables in the limit $N \rightarrow \infty$.

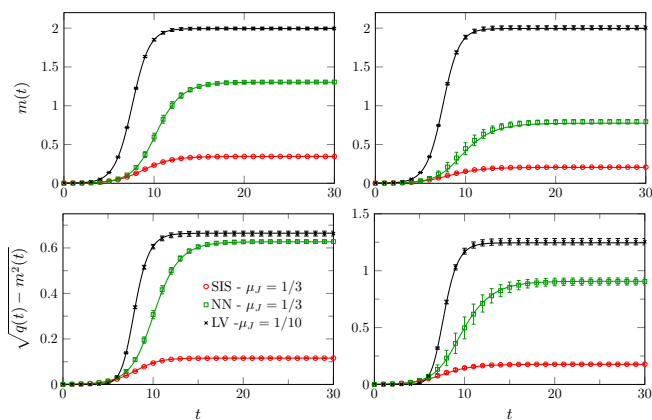


FIG. 1. Dynamics of the mean $m(t)$ and the standard deviation $\sqrt{q(t) - m^2(t)}$ for the SIS model, LV model, and NN model (see table I). Results are shown for directed random networks with average degree $c = 5$ and two indegree distributions (Eq. (9)): Poisson (left column) and geometric (right column). The distribution p_J of the coupling strengths has mean μ_J and standard deviation $\sigma_J = 0.1$. For the LV and NN models, p_J is Gaussian; for the SIS model, p_J is uniform. Solid lines are solutions of Eq. (7) using the population dynamics algorithm with 5×10^4 paths and initial condition $x_i(0) = 10^{-3}$. Symbols denote numerical simulations of Eq. (1) for an ensemble of 10 random networks generated from the configuration model with $N = 4000$ nodes. Vertical bars are the standard deviation of the macroscopic observables.

Equation (7) is formally similar to other distributional equations appearing in the study of sparse disordered systems [61–66]. Therefore, we can numerically solve this equation using the population dynamics algorithm [61, 63, 64]. In the standard version of this algorithm [61, 64], a probability density is parametrized by a population of stochastic variables. Here, we generalize the algorithm to calculate $\mathcal{P}[x]$ by introducing a population of dynamical trajectories. At each iteration step, a single path is chosen randomly from the population and updated according to the differential equation imposed by

the Dirac- δ_F in Eq. (7). After sufficient iterations, the population of paths converges to a stationary distribution, providing a numerical solution for $\mathcal{P}[x]$. A detailed account of the algorithm is in [72].

In Fig. 1, we compare the solutions of Eq. (7) with numerical simulations of the original coupled dynamics, Eq. (1), for finite N . The panels showcase the time-evolution of the mean $m(t)$ and the standard deviation $\sqrt{q(t) - m^2(t)}$ of the microscopic variables for different network topologies and three models of table I: the NN model of [1], the LV model, and the SIS model of epidemic spreading. The results in Fig. 1 are for Poisson and geometric indegrees, where $p_{\text{in},k}$ is given by

$$p_{\text{in},k} = \frac{c^k e^{-c}}{k!} \quad \text{and} \quad p_{\text{in},k} = \frac{c^k}{(c+1)^{k+1}}, \quad (9)$$

respectively. In [72], we compare the solutions of Eq. (7) with numerical simulations for two additional cases: the NN model on networks with power-law indegree distributions and the SIS model at the epidemic threshold. In all cases, the agreement between our theoretical results for $N \rightarrow \infty$ and numerical simulations for large N is excellent, confirming the exactness of Eq. (7).

An important question is whether Eq. (7) recovers the analytic results of fully-connected models as $c \rightarrow \infty$ [1, 4, 28, 30]. By taking the limit $c \rightarrow \infty$ after the thermodynamic limit $N \rightarrow \infty$, we are effectively considering the scaling regime where $c \propto N^a$, with $0 < a < 1$ [74–77]. We show in [72] that, in the limit $c \rightarrow \infty$, degree fluctuations remain significant, and $\mathcal{P}[x]$ depends on the full distribution $\nu_{\text{in}}(\kappa)$ of rescaled indegrees $\kappa_i = K_i/c$ ($i = 1, \dots, N$). The well-known effective dynamics on fully-connected networks is only recovered when $\nu_{\text{in}}(\kappa) = \delta(\kappa - 1)$. This breakdown in the universality of fully-connected models due to degree fluctuations was anticipated in [74–77].

Phase diagram of neural networks. To demonstrate the strength of Eq. (7) and its concrete applications, we derive the phase diagram of the NN model on sparse directed networks. In this context, $x_i(t) \in \mathbb{R}$ represents the synaptic current at neuron i , $f(x) = x$, and $g(x, x') = \tanh(x')$. Let us order the complex eigenvalues $\{\lambda_\alpha\}_{\alpha=1, \dots, N}$ of \mathbf{A} according to their real parts as $\text{Re}\lambda_1 \geq \text{Re}\lambda_2 \geq \dots \geq \text{Re}\lambda_N$. A linear stability analysis of Eq. (1) shows that $\mathbf{x} = 0$ is stable if $\text{Re}\lambda_1 < 1$. Based on analytic results for the spectra of directed networks for $N \rightarrow \infty$ [67–69], we find that the trivial fixed-point is stable provided $c < c_{\text{stab}}$, where

$$c_{\text{stab}} = \begin{cases} 1/\mu_J & \text{if } c > 1 + \sigma_J^2/\mu_J^2, \\ 1/(\sigma_J^2 + \mu_J^2) & \text{if } c \leq 1 + \sigma_J^2/\mu_J^2. \end{cases} \quad (10)$$

The two distinct regimes in Eq. (10) result from the gapless transition in the spectrum of \mathbf{A} [67]. For $c > 1 + \sigma_J^2/\mu_J^2$, the spectral gap $|\lambda_1 - \lambda_2|$ remains finite as $N \rightarrow$

∞ , while it vanishes for $c \leq 1 + \sigma_J^2/\mu_J^2$. Equation (10) holds for $\mu_J > 0$ and $c > 1$. The condition $c > 1$ ensures that directed networks with degree distribution $p_{k,\ell} = p_{\text{in},k}p_{\text{out},\ell}$ contain a giant strongly connected component [78, 79], implying the existence of a continuous part in the eigenvalue distribution of \mathbf{A} [68].

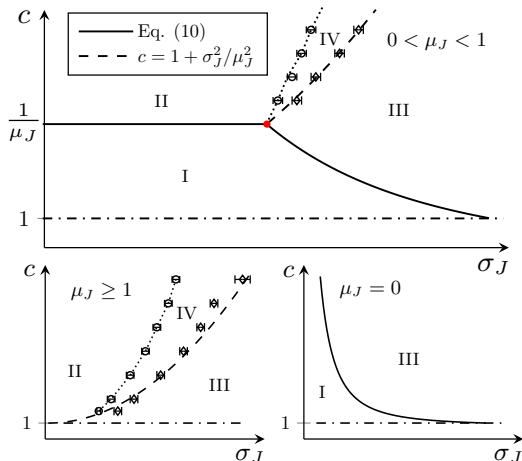


FIG. 2. Phase diagrams (c, σ_J) of the NN model for $\mu_J = 0$, $\mu_J \geq 1$, and $0 < \mu_J < 1$. The average synaptic current $m(t)$ relaxes to trivial and nontrivial fixed-points in phases I and II, respectively. In the chaotic phases III and IV, $m(t)$ exhibits aperiodic oscillations around zero and nonzero values, respectively (see Fig. 4). The dash-dotted line at $c = 1$ marks the percolation threshold, while the dashed curve identifies the gap-gapless transition. Circles and diamonds represent numerical results for the transition lines delimiting phase IV (see the main text), obtained from solutions of Eq. (7) using population dynamics with 5×10^4 paths, Poisson indegrees, and two values of μ_J ($\mu_J = 1/3$ and $\mu_J = 3/2$). The red dot marks $(c^*, \sigma_J^*) = (\mu_J^{-1}, \sqrt{\mu_J(1 - \mu_J)})$.

We emphasize that the linear stability analysis of the trivial solution provides no information about the relaxation dynamics or the stationary solutions that emerge when $\mathbf{x} = 0$ becomes unstable. Therefore, we study the dynamics and the stationary states of the NN model by solving Eq. (7). Figure 2 presents the resulting phase diagrams for different regimes of μ_J . In phase I, $m(t)$ relaxes exponentially fast to the trivial solution $m = 0$, while in phase II, $m(t)$ evolves to a nonzero fixed-point. In phases III and IV, the neural network exhibits chaotic activity, characterized by slow and aperiodic oscillations of $m(t)$ [1, 30]. The stability lines that delimit phase I are universal, as they depend only on the first and second moments of p_J and $p_{\text{in},k}$.

Figure 3 characterizes the transition between the fixed-point phases I and II. As c approaches the critical mean degree $c^* = \mu_J^{-1}$ from above, the nontrivial fixed-point $m = m(t)$ vanishes continuously. The critical point c^* is independent of $p_{\text{in},k}$ and $m(t)$ relaxes exponentially fast

inside phases I and II. Due to critical slowing down, the numerical solution of Eq. (7) becomes computationally more demanding near c^* . In phase II, the neuronal firing rates evolve to a stationary distribution with a finite variance.

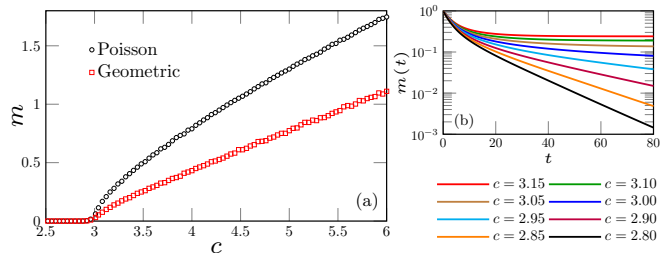


FIG. 3. Continuous transition between the fixed-point phases for the NN model on directed random networks. The coupling strengths follow a Gaussian distribution with mean $\mu_J = 1/3$ and standard deviation $\sigma_J = 0.1$. The results are derived from Eq. (7) using population dynamics with 5×10^4 paths. (a) Fixed-point solution $m(t) = m$ as a function of c for Poisson and geometric indegrees (Eq. (9)). (b) Relaxation dynamics of $m(t)$ across the transition for Poisson indegrees and initial condition $x_i(0) = 1$. For $c < \mu_J^{-1}$, $m(t)$ relaxes exponentially to $m = 0$ as $t \rightarrow \infty$.

Figure 4 shows the dynamics of $m(t)$ within the chaotic phases for several initial conditions. After a transient time T_{tr} , $m(t)$ stabilizes into an attractor, oscillating around zero in phase III and around a nonzero value in phase IV. The inset in Fig. 4(a) demonstrates the sensitivity of $m(t)$ to small perturbations in the initial conditions, characteristic of deterministic chaos [80]. By solving Eq. (7) and numerically computing the temporal averages [81]

$$M = \frac{1}{T - T_{\text{tr}}} \int_{T_{\text{tr}}}^T dt m(t), \quad (11)$$

$$\Delta^2 = \frac{1}{T - T_{\text{tr}}} \int_{T_{\text{tr}}}^T dt [M - m(t)]^2, \quad (12)$$

for $T \gg 1$, we estimate the transition lines delimiting phase IV [72]. For $T \rightarrow \infty$, the transition between phases II and IV is determined by Δ , since $\Delta = 0$ in the fixed-point phases and $\Delta > 0$ in the chaotic phases. The parameter M distinguishes the chaotic phases: $M = 0$ in phase III and $M \neq 0$ in phase IV (see Fig. 4). Our numerical results for the transition between phases III and IV are consistent with the dashed line in Fig. 2, suggesting that this transition is governed by the gap $|\lambda_1 - \lambda_2|$ in the network spectrum. Nevertheless, for $c \rightarrow \infty$ this transition to the chaotic phase III slightly deviates from the gap-gapless transition [30], particularly for large μ_J .

Conclusions. We have developed a dynamical mean-field theory of complex systems on sparse directed networks, deriving an exact path-probability equation for

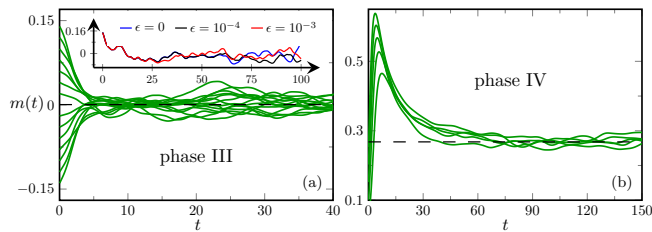


FIG. 4. Dynamics of $m(t)$ inside the chaotic phases for directed networks with Poisson indegrees and a Gaussian distribution p_J with mean $\mu_J = 1/3$. The results follow from the solutions of Eq. (7) using population dynamics with 5×10^4 paths and several initial conditions. The dashed lines indicate the value of M , Eq. (11), characterizing the chaotic attractor in each phase. (a) $c = 2.5$ and $\sigma_J = 2$. Inset: dynamics of $m(t)$ obtained from the *deterministic* Eq. (1) for a single network instance ($N = 4000$), initial condition $x_i(0) = 0.15 - \epsilon$, and different ϵ . (b) $c = 5$ and $\sigma_J = 0.62$.

the effective dynamics in the limit $N \rightarrow \infty$. Unlike sparse models with bidirected edges [38, 39], our path-probability equation can be numerically solved using population dynamics [64]. We confirmed the exactness of our general solution by comparing it with numerical simulations of fundamental models in the study of epidemic spreading, neural networks, and ecosystems. Finally, we applied our solution to determine the complete phase diagram of the sparse and directed version of the canonical neural network model of [1, 30].

The numerical solution of Eq. (7) does not require generating networks from the configuration model [71], providing moderate computational advantages over large-scale simulations of Eq. (1) on networks [22]. Beyond its numerical applications, Eq. (7) provides a foundational framework for studying the stationary states [4], computing correlation functions [3], deriving approximate dynamical equations for macroscopic order-parameters, and developing systematic perturbative approaches [26, 82].

Our work paves the way for exploring the role of sparse heterogeneous networks on the dynamics of ecosystems, coupled oscillators, epidemic spreading, and beyond. Future works include determining the phase diagram of the sparse Lotka-Volterra model [7], the influence of external noise on phase diagrams [29], and the role of network heterogeneities on the critical exponents of complex systems [77, 83]. Lastly, it would be interesting to connect the present formalism with the cavity method in [84].

F. L. M. thanks Tuan Minh Pham and Alessandro Ingrassio for many stimulating discussions. The author also thanks Thomas Peron and Tuan Minh Pham for their valuable comments on the manuscript. F. L. M. acknowledges support from CNPq (Grant No. 402487/2023-0) and the ICTP through the Associates Programme (2023-2028).

- [1] H. Sompolinsky, A. Crisanti, and H. J. Sommers, “Chaos in random neural networks,” *Phys. Rev. Lett.* **61**, 259–262 (1988).
- [2] Jonathan Kadmon and Haim Sompolinsky, “Transition to chaos in random neuronal networks,” *Phys. Rev. X* **5**, 041030 (2015).
- [3] Daniel Martí, Nicolas Brunel, and Srdjan Ostojic, “Correlations between synapses in pairs of neurons slow down dynamics in randomly connected neural networks,” *Phys. Rev. E* **97**, 062314 (2018).
- [4] A. Crisanti and H. Sompolinsky, “Path integral approach to random neural networks,” *Phys. Rev. E* **98**, 062120 (2018).
- [5] Carles Martorell, Rubén Calvo, Alessia Annibale, and Miguel A. Muñoz, “Dynamically selected steady states and criticality in non-reciprocal networks,” *Chaos, Solitons and Fractals* **182**, 114809 (2024).
- [6] Manfred Opper and Sigurd Diederich, “Phase transition and $1/f$ noise in a game dynamical model,” *Phys. Rev. Lett.* **69**, 1616–1619 (1992).
- [7] Guy Bunin, “Ecological communities with lotka-volterra dynamics,” *Phys. Rev. E* **95**, 042414 (2017).
- [8] Ada Altieri, Felix Roy, Chiara Cammarota, and Giulio Biroli, “Properties of equilibria and glassy phases of the random lotka-volterra model with demographic noise,” *Phys. Rev. Lett.* **126**, 258301 (2021).
- [9] Angélica S. Mata and Silvio C. Ferreira, “Pair quenched mean-field theory for the susceptible-infected-susceptible model on complex networks,” *Europhysics Letters* **103**, 48003 (2013).
- [10] P. Van Mieghem, “Epidemic phase transition of the sis type in networks,” *Europhysics Letters* **97**, 48004 (2012).
- [11] A. V. Goltsev, S. N. Dorogovtsev, J. G. Oliveira, and J. F. F. Mendes, “Localization and spreading of diseases in complex networks,” *Phys. Rev. Lett.* **109**, 128702 (2012).
- [12] Romualdo Pastor-Satorras, Claudio Castellano, Piet Van Mieghem, and Alessandro Vespignani, “Epidemic processes in complex networks,” *Rev. Mod. Phys.* **87**, 925–979 (2015).
- [13] J. C. Stiller and G. Radons, “Dynamics of nonlinear oscillators with random interactions,” *Phys. Rev. E* **58**, 1789–1799 (1998).
- [14] Francisco A. Rodrigues, Thomas K. DM. Peron, Peng Ji, and Jürgen Kurths, “The kuramoto model in complex networks,” *Physics Reports* **610**, 1–98 (2016), the Kuramoto model in complex networks.
- [15] Axel Prüser, Sebastian Rosmej, and Andreas Engel, “Nature of the volcano transition in the fully disordered kuramoto model,” *Phys. Rev. Lett.* **132**, 187201 (2024).
- [16] Fabian Baumann, Philipp Lorenz-Spreen, Igor M. Sokolov, and Michele Starnini, “Modeling echo chambers and polarization dynamics in social networks,” *Phys. Rev. Lett.* **124**, 048301 (2020).
- [17] Fabian Baumann, Philipp Lorenz-Spreen, Igor M. Sokolov, and Michele Starnini, “Emergence of polarized ideological opinions in multidimensional topic spaces,” *Phys. Rev. X* **11**, 011012 (2021).
- [18] Claude Godrèche and Jean-Marc Luck, “Characterising the nonequilibrium stationary states of ornstein-uhlenbeck processes,” *Journal of Physics A: Math-*

- ematical and Theoretical **52**, 035002 (2018).
- [19] Andrea Crisanti and Matteo Paoluzzi, “Most probable path of active ornstein-uhlenbeck particles,” *Phys. Rev. E* **107**, 034110 (2023).
- [20] Francesco Ferraro, Christian Grilletta, Amos Maritan, Samir Suweis, and Sandro Azaele, “Exact solution of dynamical mean-field theory for a linear system with annealed disorder,” (2024), arXiv:2405.05183 [cond-mat.dis-nn].
- [21] I.Z. Kiss, J.C. Miller, and P.L. Simon, *Mathematics of Epidemics on Networks: From Exact to Approximate Models*, Interdisciplinary Applied Mathematics (Springer International Publishing, 2017).
- [22] Diogo H. Silva, Francisco A. Rodrigues, and Silvio C. Ferreira, “High prevalence regimes in the pair-quenched mean-field theory for the susceptible-infected-susceptible model on networks,” *Phys. Rev. E* **102**, 012313 (2020).
- [23] V. Thibault, A. Allard, and P. Desrosiers, “The low-rank hypothesis of complex systems,” *Nat. Phys.* **20**, 294–302 (2024).
- [24] P. C. Martin, E. D. Siggia, and H. A. Rose, “Statistical dynamics of classical systems,” *Phys. Rev. A* **8**, 423–437 (1973).
- [25] A.C.C. Coolen, “Chapter 15 statistical mechanics of recurrent neural networks ii — dynamics,” in *Neuro-Informatics and Neural Modelling*, Handbook of Biological Physics, Vol. 4, edited by F. Moss and S. Gielen (North-Holland, 2001) pp. 619–684.
- [26] John A Hertz, Yasser Roudi, and Peter Sollich, “Path integral methods for the dynamics of stochastic and disordered systems,” *Journal of Physics A: Mathematical and Theoretical* **50**, 033001 (2016).
- [27] F Roy, G Biroli, G Bunin, and C Cammarota, “Numerical implementation of dynamical mean field theory for disordered systems: application to the lotka–volterra model of ecosystems,” *Journal of Physics A: Mathematical and Theoretical* **52**, 484001 (2019).
- [28] Tobias Galla, “Dynamically evolved community size and stability of random lotka-volterra ecosystems(a),” *Europhysics Letters* **123**, 48004 (2018).
- [29] Jannis Schuecker, Sven Goedeke, and Moritz Helias, “Optimal sequence memory in driven random networks,” *Phys. Rev. X* **8**, 041029 (2018).
- [30] Francesca Mastrogiuseppe and Srdjan Ostojic, “Linking connectivity, dynamics, and computations in low-rank recurrent neural networks,” *Neuron* **99**, 609–623.e29 (2018).
- [31] Lyle Poley, Joseph W. Baron, and Tobias Galla, “Generalized lotka-volterra model with hierarchical interactions,” *Phys. Rev. E* **107**, 024313 (2023).
- [32] Fabián Aguirre-López, “Heterogeneous mean-field analysis of the generalized lotka-volterra model on a network,” *Journal of Physics A: Mathematical and Theoretical* **57**, 345002 (2024).
- [33] Jong Il Park, Deok-Sun Lee, Sang Hoon Lee, and Hye Jin Park, “Incorporating heterogeneous interactions for ecological biodiversity,” *Phys. Rev. Lett.* **133**, 198402 (2024).
- [34] Tuan Minh Pham and Kunihiko Kaneko, “Dynamical theory for adaptive systems,” *Journal of Statistical Mechanics: Theory and Experiment* **2024**, 113501 (2024).
- [35] Valentina Ros, Felix Roy, Giulio Biroli, and Guy Bunin, “Quenched complexity of equilibria for asymmetric generalized lotka–volterra equations,” *Journal of Physics A: Mathematical and Theoretical* **56**, 305003 (2023).
- [36] M. Newman, *Networks: An Introduction* (OUP Oxford, 2010).
- [37] Paulo R. Guimarães, “The structure of ecological networks across levels of organization,” *Annual Review of Ecology, Evolution, and Systematics* **51**, 433–460 (2020).
- [38] J P L Hatchett, B Wemmenhove, I Pérez Castillo, T Nikolettopoulos, N S Skantzos, and A C C Coolen, “Parallel dynamics of disordered ising spin systems on finitely connected random graphs,” *Journal of Physics A: Mathematical and General* **37**, 6201 (2004).
- [39] I Neri and D Bollé, “The cavity approach to parallel dynamics of ising spins on a graph,” *Journal of Statistical Mechanics: Theory and Experiment* **2009**, P08009 (2009).
- [40] Kazushi Mimura and A C C Coolen, “Parallel dynamics of disordered ising spin systems on finitely connected directed random graphs with arbitrary degree distributions,” *Journal of Physics A: Mathematical and Theoretical* **42**, 415001 (2009).
- [41] Yasser Roudi and John Hertz, “Dynamical tap equations for non-equilibrium ising spin glasses,” *Journal of Statistical Mechanics: Theory and Experiment* **2011**, P03031 (2011).
- [42] Erik Aurell and Hamed Mahmoudi, “Dynamic mean-field and cavity methods for diluted ising systems,” *Phys. Rev. E* **85**, 031119 (2012).
- [43] P. Zhang, “Inference of kinetic ising model on sparse graphs,” *J. Stat. Phys.* **148**, 502–512 (2012).
- [44] Gino Del Ferraro and Erik Aurell, “Dynamic message-passing approach for kinetic spin models with reversible dynamics,” *Phys. Rev. E* **92**, 010102 (2015).
- [45] E. Aurell, G. Del Ferraro, E. Domínguez, and R. Mulet, “Cavity master equation for the continuous time dynamics of discrete-spin models,” *Phys. Rev. E* **95**, 052119 (2017).
- [46] Eduardo Domínguez Vázquez, Gino Del Ferraro, and Federico Ricci-Tersenghi, “A simple analytical description of the non-stationary dynamics in ising spin systems,” *Journal of Statistical Mechanics: Theory and Experiment* **2017**, 033303 (2017).
- [47] Giuseppe Torrisi, Alessia Annibale, and Reimer Kühn, “Overcoming the complexity barrier of the dynamic message-passing method in networks with fat-tailed degree distributions,” *Phys. Rev. E* **104**, 045313 (2021).
- [48] Giuseppe Torrisi, Reimer Kühn, and Alessia Annibale, “Uncovering the non-equilibrium stationary properties in sparse boolean networks,” *Journal of Statistical Mechanics: Theory and Experiment* **2022**, 053303 (2022).
- [49] Freya Behrens, Barbora Hudcová, and Lenka Zdeborová, “Backtracking dynamical cavity method,” *Phys. Rev. X* **13**, 031021 (2023).
- [50] Freya Behrens, Barbora Hudcová, and Lenka Zdeborová, “Dynamical phase transitions in graph cellular automata,” *Phys. Rev. E* **109**, 044312 (2024).
- [51] B. Derrida, E. Gardner, and A. Zippelius, “An exactly solvable asymmetric neural network model,” *Europhysics Letters* **4**, 167 (1987).
- [52] Malbor Asllani, Renaud Lambiotte, and Timoteo Carletti, “Structure and dynamical behavior of non-normal networks,” *Science Advances* **4**, eaau9403 (2018), <https://www.science.org/doi/pdf/10.1126/sciadv.aau9403>.
- [53] Yangfan Peng, Antje Bjelde, Pau Vilimelis Aceituno, Franz X. Mittermaier, Henrike Planert, Sabine Grosser,

- Julia Onken, Katharina Faust, Thilo Kalbhenn, Matthias Simon, Helena Radbruch, Pawel Fidzinski, Dietmar Schmitz, Henrik Alle, Martin Holtkamp, Imre Vida, Benjamin F. Grewe, and Jörg R. P. Geiger, “Directed and acyclic synaptic connectivity in the human layer 2-3 cortical microcircuit,” *Science* **384**, 338–343 (2024), <https://www.science.org/doi/pdf/10.1126/science.adg8828>.
- [54] Jennifer A. Dunne, Richard J. Williams, and Neo D. Martinez, “Food-web structure and network theory: The role of connectance and size,” *Proceedings of the National Academy of Sciences* **99**, 12917–12922 (2002), <https://www.pnas.org/doi/pdf/10.1073/pnas.192407699>.
- [55] Jordi Bascompte, “Disentangling the web of life,” *Science* **325**, 416–419 (2009), <https://www.science.org/doi/pdf/10.1126/science.1170749>.
- [56] S. S. Shen-Orr, R. Milo, S. Mangan, and U. Alon, “Network motifs in the transcriptional regulation network of *escherichia coli*,” *Nat. Genet.* **31**, 64–68 (2002).
- [57] Tong Ihn Lee, Nicola J. Rinaldi, François Robert, Duncan T. Odom, Ziv Bar-Joseph, Georg K. Gerber, Nancy M. Hannett, Christopher T. Harbison, Craig M. Thompson, Itamar Simon, Julia Zeitlinger, Ezra G. Jennings, Heather L. Murray, D. Benjamin Gordon, Bing Ren, John J. Wyrick, Jean-Bosco Tagne, Thomas L. Volkert, Ernest Fraenkel, David K. Gifford, and Richard A. Young, “Transcriptional regulatory networks in *saccharomyces cerevisiae*,” *Science* **298**, 799–804 (2002), <https://www.science.org/doi/pdf/10.1126/science.1075090>.
- [58] Haewoon Kwak, Changhyun Lee, Hosung Park, and Sue Moon, “What is twitter, a social network or a news media?” in *Proceedings of the 19th International Conference on World Wide Web* (Association for Computing Machinery, New York, NY, USA, 2010) p. 591–600.
- [59] Christoph Schweimer, Christine Gfrerer, Florian Lugstein, David Pape, Jan A. Velimsky, Robert Elsässer, and Bernhard C. Geiger, “Generating simple directed social network graphs for information spreading,” (Association for Computing Machinery, New York, NY, USA, 2022) p. 1475–1485.
- [60] R. Pastor-Satorras and A. Vespignani, *Evolution and Structure of the Internet: A Statistical Physics Approach* (Cambridge University Press, 2004).
- [61] M Mézard and G Parisi, “The bethe lattice spin glass revisited,” *Eur. Phys. J. B* **20**, 217–233 (2001).
- [62] M Mézard and G Parisi, “The cavity method at zero temperature,” *J. Stat. Phys.* **111**, 1–34 (2003).
- [63] Reimer Kühn, “Spectra of sparse random matrices,” *Journal of Physics A: Mathematical and Theoretical* **41**, 295002 (2008).
- [64] Fernando Lucas Metz, Izaak Neri, and Tim Rogers, “Spectral theory of sparse non-hermitian random matrices,” *Journal of Physics A: Mathematical and Theoretical* **52**, 434003 (2019).
- [65] R Abou-Chacra, D J Thouless, and P W Anderson, “A self-consistent theory of localization,” *Journal of Physics C: Solid State Physics* **6**, 1734 (1973).
- [66] M. Mézard and A. Montanari, *Information, Physics, and Computation*, Oxford Graduate Texts (OUP Oxford, 2009).
- [67] Izaak Neri and Fernando Lucas Metz, “Eigenvalue outliers of non-hermitian random matrices with a local tree structure,” *Phys. Rev. Lett.* **117**, 224101 (2016).
- [68] Izaak Neri and Fernando Lucas Metz, “Linear stability analysis of large dynamical systems on random directed graphs,” *Phys. Rev. Res.* **2**, 033313 (2020).
- [69] Fernando Lucas Metz and Izaak Neri, “Localization and universality of eigenvectors in directed random graphs,” *Phys. Rev. Lett.* **126**, 040604 (2021).
- [70] M. E. J. Newman, S. H. Strogatz, and D. J. Watts, “Random graphs with arbitrary degree distributions and their applications,” *Phys. Rev. E* **64**, 026118 (2001).
- [71] Bailey K. Fosdick, Daniel B. Larremore, Joel Nishimura, and Johan Ugander, “Configuring random graph models with fixed degree sequences,” *SIAM Review* **60**, 315–355 (2018), <https://doi.org/10.1137/16M1087175>.
- [72] See the Supplemental Material for all derivations of DMFT and a detailed account of the population dynamics algorithm.
- [73] Charles Bordenave and Marc Lelarge, “Resolvent of large random graphs,” *Random Structures & Algorithms* **37**, 332–352 (2010), <https://onlinelibrary.wiley.com/doi/pdf/10.1002/rsa.20313>.
- [74] Fernando L. Metz and Jeferson D. Silva, “Spectral density of dense random networks and the breakdown of the wigner semicircle law,” *Phys. Rev. Res.* **2**, 043116 (2020).
- [75] Fernando L Metz and Thomas Peron, “Mean-field theory of vector spin models on networks with arbitrary degree distributions,” *Journal of Physics: Complexity* **3**, 015008 (2022).
- [76] Jeferson D Silva and Fernando L Metz, “Analytic solution of the resolvent equations for heterogeneous random graphs: spectral and localization properties,” *Journal of Physics: Complexity* **3**, 045012 (2022).
- [77] Leonardo S. Ferreira and Fernando L. Metz, “Nonequilibrium dynamics of the ising model on heterogeneous networks with an arbitrary distribution of threshold noise,” *Phys. Rev. E* **107**, 034127 (2023).
- [78] G. Timár, A. V. Goltsev, S. N. Dorogovtsev, and J. F. F. Mendes, “Mapping the structure of directed networks: Beyond the bow-tie diagram,” *Phys. Rev. Lett.* **118**, 078301 (2017).
- [79] Ivan Kryven, “Emergence of the giant weak component in directed random graphs with arbitrary degree distributions,” *Phys. Rev. E* **94**, 012315 (2016).
- [80] G.L. Baker and J.P. Gollub, *Chaotic Dynamics: An Introduction* (Cambridge University Press, 1996).
- [81] Maximilian Gelbrecht, Jürgen Kurths, and Frank Hellmann, “Monte carlo basin bifurcation analysis,” *New Journal of Physics* **22**, 033032 (2020).
- [82] F. L. Metz, G. Parisi, and L. Leuzzi, “Finite-size corrections to the spectrum of regular random graphs: An analytical solution,” *Phys. Rev. E* **90**, 052109 (2014).
- [83] Thibaut Arnoult de Pirey and Guy Bunin, “Critical behavior of a phase transition in the dynamics of interacting populations,” (2024), arXiv:2402.05063 [cond-mat.stat-mech].
- [84] Mattia Tarabolo and Luca Dall’Asta, “Gaussian approximation of dynamic cavity equations for linearly-coupled stochastic dynamics,” (2024), arXiv:2406.14200 [cond-mat.dis-nn].

Supplemental material for “Dynamical Mean-Field Theory of Complex Systems on
Sparse Directed Networks”

Fernando L. Metz

Physics Institute, Federal University of Rio Grande do Sul, 91501-970 Porto Alegre, Brazil

(Dated: January 23, 2025)

arXiv:2406.06346v2 [cond-mat.dis-nn] 21 Jan 2025

I. INTRODUCTION

In this supplemental material, we show how to apply dynamical mean-field theory (DMFT) to solve nonlinear systems of coupled differential equations governing a broad range of dynamical processes on sparse directed graphs. The microscopic variables $x_1(t), \dots, x_N(t)$ evolve in time according to the coupled differential equations

$$\dot{x}_i(t) = -f(x_i) + \sum_{j=1}^N C_{ij} J_{ij} g(x_i, x_j) + h_i(t) + \xi_i(t), \quad (1)$$

with $i = 1, \dots, N$. The variable $\xi_i(t)$ represents an uncorrelated Gaussian noise with mean zero and variance σ^2 (in the main text, we present results for $\xi_i(t) = 0$). Unlike the model definitions in the main text, here we have included, for technical purposes, an external field $h_i(t)$ in the dynamical equations, which will be set to zero at the end of the calculation. The functions $f(x)$ and $g(x, x')$ specify the model under study. Table I of the main text shows five paradigmatic examples of complex systems modeled by Eq. (1).

The binary variable $C_{ij} \in \{0, 1\}$ tells us whether there is a directed edge pointing from node j to node i in the network, while J_{ij} represents the strength of the directed interaction $j \rightarrow i$. We set $C_{ii} = 0$. The off-diagonal entries $\{C_{ij}\}_{i \neq j}$ encode the network topology, and they are drawn from the joint probability distribution

$$\mathbb{P}(\{C_{ij}\}) = \frac{1}{\mathcal{N}} \prod_{i \neq j=1}^N \left[\frac{c}{N} \delta_{C_{ij}, 1} + \left(1 - \frac{c}{N}\right) \delta_{C_{ij}, 0} \right] \prod_{i=1}^N \delta_{K_i, \sum_{j=1}^N C_{ij}} \delta_{L_i, \sum_{j=1}^N C_{ji}}, \quad (2)$$

where \mathcal{N} is the normalization factor. The local variables $K_i = \sum_{j=1}^N C_{ij}$ and $L_i = \sum_{j=1}^N C_{ji}$ denote, respectively, the indegree and the outdegree of node i . The joint probability distribution of indegrees k and outdegrees ℓ is formally defined as

$$p_{k,\ell} = \lim_{N \rightarrow \infty} \frac{1}{N} \sum_{i=1}^N \delta_{K_i, k} \delta_{L_i, \ell}, \quad (3)$$

while the mean degree c is given by

$$c = \sum_{k,\ell=0}^{\infty} k p_{k,\ell} = \sum_{k,\ell=0}^{\infty} \ell p_{k,\ell}. \quad (4)$$

The parameter c controls the average number of links that enter or leave a node. The distribution of Eq. (2) defines an ensemble of directed random networks in which a directed link $j \rightarrow i$ is randomly placed between nodes i and j with probability c/N , subject to the local constraints imposed by the prescribed degree sequences K_1, \dots, K_N and L_1, \dots, L_N .

The degrees at different nodes are independent and identically distributed random variables drawn from the joint distribution $p_{k,\ell}$. However, the pair of degrees (K_i, L_i) at node i might be correlated. If K_i and L_i are statistically independent, then the joint degree distribution $p_{k,\ell}$ factorizes as $p_{k,\ell} = p_{\text{in},k} p_{\text{out},\ell}$. Here we solve the dynamics for an arbitrary $p_{k,\ell}$, while in the main text we present the final solution for the factorized case $p_{k,\ell} = p_{\text{in},k} p_{\text{out},\ell}$. The coupling strengths $\{J_{ij}\}$ are independent and identically distributed random variables drawn from an arbitrary distribution p_J with mean μ_J and variance σ_J^2 . Thus, the distributions $p_{k,\ell}$ and p_J fully specify the ensemble of networks.

In the next section, we detail how to solve the current model, in the limit $N \rightarrow \infty$, using dynamical mean-field theory (DMFT). We emphasize that we solve the model for *finite* c , which characterizes a genuine sparse interacting system, where the average number of edges per node remains finite in the thermodynamic limit. As we show below, the main outcome of DMFT for finite c is a self-consistent equation for the path-probability $\mathcal{P}[x]$ encoding the effective dynamics of a single dynamical variable. The solution of this equation not only allows to compute macroscopic observables, but it also enables to follow the time-evolution of the full probability distribution of the microscopic degrees of freedom. In section III, we explain how to generalize the population dynamics algorithm [1–3] to solve the self-consistent equation for the path-probability $\mathcal{P}[x]$. We also present a detailed account of this algorithm, which we hope will be useful for future works, and we explain how to estimate the transition lines in Fig. 2 of the main text. Finally, in section IV, we calculate the high-connectivity limit $c \rightarrow \infty$ of $\mathcal{P}[x]$ and discuss its convergence towards fully-connected models. In particular, we show that the expression for $\mathcal{P}[x]$ of fully-connected models is only recovered if the variance of rescaled degrees goes to zero. In other words, the dynamics of fully-connected models is not universal with respect to degree fluctuations.

II. DYNAMICAL MEAN-FIELD THEORY FOR MODELS ON SPARSE DIRECTED NETWORKS

In this section we explain how to solve the dynamics of the model in the limit $N \rightarrow \infty$ using dynamical mean-field theory. Let $\mathbf{x}(t) = (x_1(t), \dots, x_N(t))$ denotes the global state of the system at time t , and let $\mathcal{P}[\mathbf{x}]$ be the functional probability density of observing a continuous trajectory of the global state $\mathbf{x}(t)$ in a finite time interval. By defining the distribution $p_0(\mathbf{x}(0))$ of the initial state $\mathbf{x}(0)$, the path-probability $\mathcal{P}[\mathbf{x}]$ can be formally written as

$$\mathcal{P}[\mathbf{x}] = p_0(\mathbf{x}(0)) \int \left(\prod_{i=1}^N D\xi_i \right) \mathcal{P}_\sigma[\boldsymbol{\xi}] \prod_{i=1}^N \delta_F \left[\dot{x}_i + f(x_i) - \sum_{j=1}^N C_{ij} J_{ij} g(x_i, x_j) - h_i(t) + \xi_i(t) \right], \quad (5)$$

where δ_F is a Dirac- δ functional, and the generic symbol Dy represents a functional integration measure over all possible functions $y(t)$ in the prescribed time domain. The object $\mathcal{P}_\sigma[\boldsymbol{\xi}]$ is the path-probability of the Gaussian noise

$$\mathcal{P}_\sigma[\boldsymbol{\xi}] = \frac{1}{\mathcal{N}_\sigma} \exp \left(-\frac{1}{2\sigma^2} \int dt \sum_{i=1}^N (\xi_i(t))^2 \right), \quad (6)$$

with \mathcal{N}_σ the normalization constant. The integrals over time run over a fixed time interval, but we omit the limits of integration, here and elsewhere, for the sake of simplifying the notation. The starting point of DMFT is the introduction of the generating functional $\mathcal{Z}[\boldsymbol{\psi}, \mathbf{h}]$ of the path-probability $\mathcal{P}[\mathbf{x}]$,

$$\mathcal{Z}[\boldsymbol{\psi}, \mathbf{h}] = \int \left(\prod_{i=1}^N Dx_i \right) \mathcal{P}[\mathbf{x}] e^{i \int dt \sum_{i=1}^N x_i(t) \psi_i(t)}, \quad (7)$$

where $\boldsymbol{\psi}(t) = (\psi_1(t), \dots, \psi_N(t))$ and $\mathbf{h}(t) = (h_1(t), \dots, h_N(t))$. The derivatives of $\mathcal{Z}[\boldsymbol{\psi}, \mathbf{h}]$ with respect to the sources $\psi_1(t), \dots, \psi_N(t)$ yield the average of products of $x_1(t), \dots, x_N(t)$ over the dynamical process specified by Eq. (1). For instance, the moments of $x_i(t)$ in the absence of external fields ($h_i(t) = 0$) follow from

$$\langle x_i^n(t) \rangle = (-i)^n \lim_{\boldsymbol{\psi} \rightarrow 0} \lim_{\mathbf{h} \rightarrow 0} \frac{\delta^n \mathcal{Z}[\boldsymbol{\psi}, \mathbf{h}]}{\delta \psi_i^n(t)}. \quad (8)$$

In particular, the first two moments yield the time-evolution of the following macroscopic observables

$$m(t) = \lim_{N \rightarrow \infty} \frac{1}{N} \sum_{i=1}^N \langle x_i(t) \rangle, \quad (9)$$

$$q(t) = \lim_{N \rightarrow \infty} \frac{1}{N} \sum_{i=1}^N \langle x_i^2(t) \rangle. \quad (10)$$

By construction, the generating functional fulfills the normalization condition $\mathcal{Z}[0, \mathbf{h}] = 1$.

By inserting Eq. (5) into the definition of $\mathcal{Z}[\boldsymbol{\psi}, \mathbf{h}]$, using a functional integral representation of δ_F , and then integrating over the Gaussian noise $\boldsymbol{\xi}(t)$, we obtain the following expression

$$\begin{aligned} \mathcal{Z}[\boldsymbol{\psi}, \mathbf{h}] &= \int \left(\prod_{i=1}^N Dx_i D\hat{x}_i \right) p_0(\mathbf{x}(0)) \exp \left(-i \sum_{i \neq j=1}^N C_{ij} J_{ij} \int dt \hat{x}_i(t) g(x_i(t), x_j(t)) \right) \\ &\times \exp \left(i \int dt \sum_{i=1}^N S_i(x_i(t), \hat{x}_i(t), \psi_i(t), h_i(t)) \right), \end{aligned} \quad (11)$$

where the single-site action S_i is defined as

$$S_i[x_i(t), \hat{x}_i(t), \psi_i(t), h_i(t)] = x_i(t) \psi_i(t) + \frac{i\sigma}{2} \hat{x}_i^2(t) + \hat{x}_i(t) [\dot{x}_i(t) + f(x_i(t)) - h_i(t)]. \quad (12)$$

According to Eq. (11), the external sources $h_i(t)$ and $\psi_i(t)$ are coupled, respectively, to the dynamical variables $\hat{x}_i(t)$ and $x_i(t)$ at node i . Both fields $h_i(t)$ and $\psi_i(t)$ are important to simplify the saddle-point equations and identify the physical meaning of the order-parameters.

A. The saddle-point integral

The aim of DMFT is to compute, in the limit $N \rightarrow \infty$, the disorder averaged generating functional, $\langle \mathcal{Z}[\boldsymbol{\psi}, \mathbf{h}] \rangle_{\{C_{ij}, J_{ij}\}}$. The symbol $\langle \dots \rangle_{\{C_{ij}, J_{ij}\}}$ represents the average over both the graph structure $\{C_{ij}\}$ and the coupling strengths $\{J_{ij}\}$. In this subsection, we explain how to reduce the calculation of $\langle \mathcal{Z}[\boldsymbol{\psi}, \mathbf{h}] \rangle_{\{C_{ij}, J_{ij}\}}$ to the solution of a saddle-point integral in the limit $N \rightarrow \infty$.

By taking the average of Eq. (11) over $\{C_{ij}\}$ and $\{J_{ij}\}$, we can write $\langle \mathcal{Z}[\boldsymbol{\psi}, \mathbf{h}] \rangle_{\{C_{ij}, J_{ij}\}}$ as follows

$$\langle \mathcal{Z}[\boldsymbol{\psi}, \mathbf{h}] \rangle_{\{C_{ij}, J_{ij}\}} = \int \left(\prod_{i=1}^N Dx_i D\hat{x}_i \right) p_0(\mathbf{x}(0)) \mathcal{F}[\mathbf{x}, \hat{\mathbf{x}}] \exp \left(i \int dt \sum_{i=1}^N S_i(x_i(t), \hat{x}_i(t), \psi_i(t), h_i(t)) \right), \quad (13)$$

where

$$\mathcal{F}[\mathbf{x}, \hat{\mathbf{x}}] = \left\langle \prod_{i \neq j=1}^N \exp \left(-i C_{ij} J_{ij} \int dt \hat{x}_i(t) g(x_i(t), x_j(t)) \right) \right\rangle_{\{C_{ij}, J_{ij}\}}. \quad (14)$$

By using the integral representation of the Kronecker- δ

$$\delta_{n,m} = \int_0^{2\pi} \frac{du}{2\pi} \exp[iu(n-m)] \quad (n, m \in \mathbb{N}), \quad (15)$$

we can factorize the joint distribution $\mathbb{P}(\{C_{ij}\})$, Eq. (2), in terms of a product over pairs of nodes

$$\mathbb{P}(\{C_{ij}\}) = \frac{1}{N} \int_0^{2\pi} \left(\frac{du_i dv_i}{4\pi^2} \right) e^{i \sum_{i=1}^N (K_i u_i + L_i v_i)} \prod_{i \neq j=1}^N \left[\frac{c}{N} \delta_{C_{ij}, 1} + \left(1 - \frac{c}{N} \right) \delta_{C_{ij}, 0} \right] e^{-C_{ij}(u_i + v_j)}. \quad (16)$$

This expression for $\mathbb{P}(\{C_{ij}\})$ allows us to calculate the average over $\{C_{ij}\}$ in Eq. (14), leading to the result

$$\mathcal{F}[\mathbf{x}, \hat{\mathbf{x}}] \simeq \int_0^{2\pi} \left(\prod_{i=1}^N \frac{du_i dv_i}{4\pi^2} \right) \exp \left(i \sum_{i=1}^N (u_i K_i + v_i L_i) + \frac{c}{N} \sum_{i \neq j=1}^N e^{-i(u_i + v_j)} \left\langle e^{-iJ \int dt \hat{x}_i(t) g(x_i(t), x_j(t))} \right\rangle_J \right), \quad (17)$$

valid for large N . We have retained only terms of $\mathcal{O}(N)$ in the exponent of Eq. (17), since these are precisely the terms that will contribute to the solution of the saddle-point integral for $N \rightarrow \infty$. In addition, irrelevant terms that arise from the normalization factor in Eq. (2) and which are independent of $\{\hat{x}_i(t), x_i(t)\}$ have been neglected when writing Eq. (17). The symbol $\langle \dots \rangle_J$ denotes the average over the coupling strength J between a single pair of nodes.

In contrast to fully-connected Gaussian models, where the disorder average of $\mathcal{Z}[\boldsymbol{\psi}, \mathbf{h}]$ yields a quadratic functional of the dynamical variables [4, 5], here the exponent in Eq. (17) contains an exponential functional of $\{\hat{x}_i(t), x_i(t)\}$. This non-quadratic behaviour renders the problem technically more challenging in comparison to fully-connected models. In spite of that, we can still decouple sites by introducing the functional order-parameters

$$P[x] = \frac{1}{N} \sum_{i=1}^N \delta_F[x(t) - x_i(t)] e^{-iv_i}, \quad (18)$$

$$W[x, \hat{x}] = \frac{1}{N} \sum_{i=1}^N \delta_F[x(t) - x_i(t)] \delta_F[\hat{x}(t) - \hat{x}_i(t)] e^{-iu_i}. \quad (19)$$

Indeed, substituting Eq. (17) in Eq. (13), we can write $\langle \mathcal{Z}[\boldsymbol{\psi}, \mathbf{h}] \rangle_{\{C_{ij}, J_{ij}\}}$ as a functional integral over $P[x]$ and $W[x, \hat{x}]$, namely

$$\begin{aligned} \langle \mathcal{Z}[\boldsymbol{\psi}, \mathbf{h}] \rangle_{\{C_{ij}, J_{ij}\}} &\simeq \int \left(\prod_{i=1}^N Dx_i D\hat{x}_i \right) p_0(\mathbf{x}(0)) \int_0^{2\pi} \left(\prod_{i=1}^N \frac{du_i dv_i}{4\pi^2} \right) e^{i \int dt \sum_{i=1}^N S_i(x_i(t), \hat{x}_i(t), \psi_i(t), h_i(t)) + i \sum_{i=1}^N (u_i K_i + v_i L_i)} \\ &\times \int DP DW \delta_F \left[P[x] - \frac{1}{N} \sum_{i=1}^N \delta_F[x(t) - x_i(t)] e^{-iv_i} \right] \delta_F \left[W[x, \hat{x}] - \frac{1}{N} \sum_{i=1}^N \delta_F[x(t) - x_i(t)] \delta_F[\hat{x}(t) - \hat{x}_i(t)] e^{-iu_i} \right] \\ &\times \exp \left(cN \int Dx D\hat{x}' D\hat{x} W[x, \hat{x}] P[x'] \left\langle e^{-iJ \int dt \hat{x}(t) g(x(t), x'(t))} \right\rangle_J \right). \end{aligned} \quad (20)$$

By assuming that the distribution of the initial state factorizes as $p_0(\mathbf{x}(0)) = \prod_{i=1}^N p_0(x_i(0))$, and introducing the conjugate order-parameters $\hat{P}[x]$ and $\hat{W}[x, \hat{x}]$ by means of the functional Fourier transforms,

$$\begin{aligned} \delta_F \left[P[x] - \frac{1}{N} \sum_{i=1}^N \delta_F [x(t) - x_i(t)] e^{-iv_i} \right] &= \int D\hat{P} e^{i \int D x \hat{P}[x] P[x] - \frac{i}{N} \sum_{i=1}^N \hat{P}[x_i] e^{-iv_i}}, \\ \delta_F \left[W[x, \hat{x}] - \frac{1}{N} \sum_{i=1}^N \delta_F [x(t) - x_i(t)] \delta_F [\hat{x}(t) - \hat{x}_i(t)] e^{-iu_i} \right] &= \int D\hat{W} e^{i \int D x D \hat{x} \hat{W}[x, \hat{x}] W[x, \hat{x}] - \frac{i}{N} \sum_{i=1}^N \hat{W}[x_i, \hat{x}_i] e^{-iu_i}}, \end{aligned}$$

we are able to factorize the exponent of Eq. (20) as a sum of single-site functionals, yielding

$$\langle \mathcal{Z}[\boldsymbol{\psi}, \mathbf{h}] \rangle_{\{C_{ij}, J_{ij}\}} \simeq \int D P D \hat{P} D W D \hat{W} \exp \left(i \int D x \hat{P}[x] P[x] + i \int D x D \hat{x} \hat{W}[x, \hat{x}] W[x, \hat{x}] \right) \quad (21)$$

$$\begin{aligned} &\times \exp \left(c N \int D x D x' D \hat{x} W[x, \hat{x}] P[x'] \left\langle e^{-iJ \int dt \hat{x}(t) g(x(t), x'(t))} \right\rangle_J \right) \\ &\times \exp \left[\sum_{i=1}^N \ln \left(\int D x D \hat{x} p_0(x(0)) \int_0^{2\pi} \frac{d u d v}{4\pi^2} e^{i \int dt S_i(x(t), \hat{x}(t), \psi_i(t), h_i(t)) + i(u K_i + v L_i) - \frac{i}{N} e^{-iv} \hat{P}[x] - \frac{i}{N} e^{-iu} \hat{W}[x, \hat{x}]} \right) \right]. \quad (22) \end{aligned}$$

Finally, we use the power-series representations

$$\exp \left(-\frac{i}{N} e^{-iv} \hat{P}[x] \right) = \sum_{r=0}^{\infty} \frac{1}{r!} \left(-\frac{i}{N} \right)^r \left(\hat{P}[x] \right)^r e^{-ivr} \quad (23)$$

and

$$\exp \left(-\frac{i}{N} e^{-iu} \hat{W}[x, \hat{x}] \right) = \sum_{r=0}^{\infty} \frac{1}{r!} \left(-\frac{i}{N} \right)^r \left(\hat{W}[x, \hat{x}] \right)^r e^{-iur}, \quad (24)$$

which enables to integrate over u and v in Eq. (22). By rescaling the conjugate order-parameters in the resulting expression as $\hat{P}[x] \rightarrow N\hat{P}[x]$ and $\hat{W}[x, \hat{x}] \rightarrow N\hat{W}[x, \hat{x}]$, we can express $\langle \mathcal{Z}[\boldsymbol{\psi}, \mathbf{h}] \rangle_{\{C_{ij}, J_{ij}\}}$ as an integral over the order-parameters

$$\langle \mathcal{Z}[\boldsymbol{\psi}, \mathbf{h}] \rangle_{\{C_{ij}, J_{ij}\}} \simeq \int D P D \hat{P} D W D \hat{W} e^{N\Phi[P, \hat{P}, W, \hat{W}]}, \quad (25)$$

with

$$\begin{aligned} \Phi[P, \hat{P}, W, \hat{W}] &= i \int D x \hat{P}[x] P[x] + i \int D x D \hat{x} \hat{W}[x, \hat{x}] W[x, \hat{x}] + c \int D x D x' D \hat{x} W[x, \hat{x}] P[x'] \left\langle e^{-iJ \int dt \hat{x}(t) g(x(t), x'(t))} \right\rangle_J \\ &+ \frac{1}{N} \sum_{i=1}^N \ln \left[\int D x D \hat{x} p_0(x(0)) e^{i \int dt S_i(x(t), \hat{x}(t), \psi_i(t), h_i(t))} \left(-i\hat{P}[x] \right)^{L_i} \left(-i\hat{W}[x, \hat{x}] \right)^{K_i} \right]. \quad (26) \end{aligned}$$

The above expression for Φ omits an additive constant that is independent of the order-parameters. Now we can find the asymptotic behaviour of the integral in Eq. (25) using the saddle-point method. In the limit $N \rightarrow \infty$, the integral is dominated by the stationary points of $\Phi[P, \hat{P}, W, \hat{W}]$,

$$\langle \mathcal{Z}[\boldsymbol{\psi}, \mathbf{h}] \rangle_{\{C_{ij}, J_{ij}\}} \simeq e^{N\Phi[P_s, \hat{P}_s, W_s, \hat{W}_s]}, \quad (27)$$

where the functional order-parameters that extremize $\Phi[P, \hat{P}, W, \hat{W}]$ fulfill the saddle-point equations

$$P_s[x] = \frac{1}{N} \sum_{i=1}^N \frac{L_i}{B_i[h_i, \psi_i]} p_0(x(0)) \left(-i\hat{P}_s[x] \right)^{L_i-1} \int D \hat{x} \left(-i\hat{W}_s[x, \hat{x}] \right)^{K_i} e^{i \int dt S_i(x(t), \hat{x}(t), \psi_i(t), h_i(t))}, \quad (28)$$

$$W_s[x, \hat{x}] = \frac{1}{N} \sum_{i=1}^N \frac{K_i}{B_i[h_i, \psi_i]} p_0(x(0)) \left(-i\hat{W}_s[x, \hat{x}] \right)^{K_i-1} \left(-i\hat{P}_s[x] \right)^{L_i} e^{i \int dt S_i(x(t), \hat{x}(t), \psi_i(t), h_i(t))}, \quad (29)$$

$$\hat{P}_s[x] = ic \int D x' D \hat{x} W_s[x', \hat{x}] \left\langle e^{-iJ \int dt \hat{x}(t) g(x'(t), x(t))} \right\rangle_J, \quad (30)$$

$$\hat{W}_s[x, \hat{x}] = ic \int D x' P_s[x'] \left\langle e^{-iJ \int dt \hat{x}(t) g(x(t), x'(t))} \right\rangle_J, \quad (31)$$

with

$$B_i[h_i, \psi_i] = \int Dx D\hat{x} p_0(x(0)) e^{i \int dt S_i(x(t), \hat{x}(t), \psi_i(t), h_i(t))} \left(-i\hat{P}_s[x]\right)^{L_i} \left(-i\hat{W}_s[x, \hat{x}]\right)^{K_i}. \quad (32)$$

The self-consistent Eqs. (28-31) are derived from the application of the stationarity conditions

$$\left. \frac{\delta \Phi}{\delta P[x]} \right|_s = \left. \frac{\delta \Phi}{\delta \hat{P}[x]} \right|_s = \left. \frac{\delta \Phi}{\delta W[x, \hat{x}]} \right|_s = \left. \frac{\delta \Phi}{\delta \hat{W}[x, \hat{x}]} \right|_s = 0, \quad (33)$$

where the notation $(\dots)|_s$ means that $P[x] = P_s[x]$, $\hat{P}[x] = \hat{P}_s[x]$, $W[x, \hat{x}] = W_s[x, \hat{x}]$ and $\hat{W}[x, \hat{x}] = \hat{W}_s[x, \hat{x}]$.

B. Physical interpretation of the order-parameters

In this subsection we explain how to distill the physical interpretation of the functional order-parameters, which plays an important role in simplifying the saddle-point equations. In addition, we show how Eqs. (28-31) can be reduced to a pair of self-consistent equations for the path-probability that determines the effective dynamics of a single degree of freedom.

First, we set $\psi_i(t) = h_i(t) = 0$ in the single-site action $S_i[x(t), \hat{x}(t), \psi_i(t), h_i(t)]$ (see Eq. (12)) and define the following normalized functional

$$\gamma[x, \hat{x}|k, \ell] = \frac{p_0(x(0)) e^{i \int dt S(x(t), \hat{x}(t))} \left(-i\hat{P}_s[x]\right)^\ell \left(-i\hat{W}_s[x, \hat{x}]\right)^k}{\int Dx D\hat{x} p_0(x(0)) e^{i \int dt S(x(t), \hat{x}(t))} \left(-i\hat{P}_s[x]\right)^\ell \left(-i\hat{W}_s[x, \hat{x}]\right)^k} \quad (34)$$

for fixed indegree k and outdegree ℓ . Our first task is to find out what is the physical interpretation of the above object. With that in mind, we take the derivative of Eq. (27) with respect to $\psi_i(t)$ and then we set $\psi_i(t) = h_i(t) = 0$, namely

$$\lim_{h \rightarrow 0} \lim_{\psi \rightarrow 0} \frac{\delta \langle \mathcal{Z}[\boldsymbol{\psi}, \mathbf{h}] \rangle_{\{C_{ij}, J_{ij}\}}}{\delta \psi_i(t)} = i \int Dx D\hat{x} x(t) \gamma[x, \hat{x}|K_i, L_i]. \quad (35)$$

Comparing the above expression with the first moment $\langle x_i(t) \rangle$ defined in Eq. (8), we conclude that

$$\mathcal{P}[x|k, \ell] = \int D\hat{x} \gamma[x, \hat{x}|k, \ell] \quad (36)$$

is the path-probability describing the effective dynamics of a single variable $x(t)$ conditioned to the indegree k and outdegree ℓ . Clearly, the path-probability $\mathcal{P}[x]$ of observing a dynamical trajectory of $x(t)$ is obtained by averaging $\mathcal{P}[x|k, \ell]$ over the joint degree distribution

$$\mathcal{P}[x] = \sum_{k, \ell=0}^{\infty} p_{k, \ell} \mathcal{P}[x|k, \ell]. \quad (37)$$

Equation (37) defines the central object of dynamical mean-field theory, as $\mathcal{P}[x]$ determines the effective dynamics of a single degree of freedom in the thermodynamic limit $N \rightarrow \infty$.

Let us derive a self-consistent equation for $\mathcal{P}[x]$. The first step consists in relating the functional probability densities, $\mathcal{P}[x|k, \ell]$ and $\gamma[x, \hat{x}|k, \ell]$, to the functional order-parameters using the saddle-point equations of the previous section. By setting $\psi_i(t) = h_i(t) = 0$ in Eqs. (28) and (30), we obtain the following relation

$$-iP_s[x] \hat{P}_s[x] = \sum_{k, \ell=0}^{\infty} \ell p_{k, \ell} \mathcal{P}[x|k, \ell]. \quad (38)$$

Similarly, combining Eqs. (29) and (31) for $\psi_i(t) = h_i(t) = 0$, we find

$$-iW_s[x, \hat{x}] \hat{W}_s[x, \hat{x}] = \sum_{k, \ell=0}^{\infty} k p_{k, \ell} \gamma[x, \hat{x}|k, \ell]. \quad (39)$$

Let us now see how the saddle-point equations simplify in the case of directed networks. By introducing the Fourier transform of $W_s[x, \hat{x}]$,

$$R_s[x|\theta] = \int D\hat{x} e^{-i \int dt \hat{x}(t)\theta(t)} W_s[x, \hat{x}], \quad (40)$$

we rewrite Eq. (30) as follows

$$\hat{P}_s[x] = ic \int Dx' \left\langle R_s[x'|Jg(x', x)] \right\rangle_J. \quad (41)$$

Using the definition of $W_s[x, \hat{x}]$, Eq. (19), we write $R_s[x|\theta]$ as

$$R_s[x|\theta] = \frac{1}{N} \sum_{i=1}^N \delta_F[x(t) - x_i(t)] e^{-iu_i - i \int dt \hat{x}_i(t)\theta(t)}. \quad (42)$$

Building on the DMFT for the dynamics of binary-state variables on directed random graphs [6, 7], we can compute the average of the above expression over $\{x_i(t), \hat{x}_i(t), u_i\}_{i=1}^N$, with the weight defined by Eq. (22), and show that

$$\int Dx R_s[x|\theta] = 1 \quad (43)$$

for arbitrary $\theta(t)$. Thus, from Eqs. (41) and (43), we conclude that

$$\hat{P}_s[x] = ic, \quad (44)$$

which allows us to simplify the saddle-point equations. The above expression for $\hat{P}_s[x]$ only holds for networks without bidirected edges [6, 7]. Now we can identify the physical meaning of the order-parameter $P_s[x]$. Substituting Eq. (44) in Eqs. (36) and (38), we obtain

$$P_s[x] = \sum_{k, \ell=0}^{\infty} \frac{\ell p_{k, \ell}}{c} \mathcal{P}[x|k], \quad (45)$$

where $\mathcal{P}[x|k]$ is given by

$$\mathcal{P}[x|k] = \int \left(\prod_{j=1}^k Dx_j P_s[x_j] \right) \int \left(\prod_{j=1}^k dJ_j p_J(J_j) \right) \int D\xi \mathcal{P}_\sigma[\xi] \delta_F \left[\dot{x}(t) + f(x(t)) - \sum_{j=1}^k J_j g(x(t), x_j(t)) - \xi(t) \right]. \quad (46)$$

We have absorbed the distribution $p_0(x(0))$ of the initial state in the definition of $\delta_F[\dots]$, which constrains the effective dynamics of $x(t)$. Note, from Eq. (45), that $P_s[x]$ is the average of the conditioned path-probability $\mathcal{P}[x|k]$ over the degrees k and ℓ with the joint distribution $\frac{\ell p_{k, \ell}}{c}$. Equations (45) and (46) lead to the self-consistent equation for $P_s[x]$

$$P_s[x] = \sum_{k, \ell=0}^{\infty} \frac{\ell p_{k, \ell}}{c} \int \left(\prod_{j=1}^k Dx_j P_s[x_j] \right) \int \left(\prod_{j=1}^k dJ_j p_J(J_j) \right) \int D\xi \mathcal{P}_\sigma[\xi] \delta_F \left[\dot{x}(t) + f(x(t)) - \sum_{j=1}^k J_j g(x(t), x_j(t)) - \xi(t) \right]. \quad (47)$$

Once we determine $P_s[x]$ from the solutions of the above equation, the path-probability $\mathcal{P}[x]$ follows from Eqs. (37) and (46), namely

$$\mathcal{P}[x] = \sum_{k, \ell=0}^{\infty} p_{k, \ell} \int \left(\prod_{j=1}^k Dx_j P_s[x_j] \right) \int \left(\prod_{j=1}^k dJ_j p_J(J_j) \right) \int D\xi \mathcal{P}_\sigma[\xi] \delta_F \left[\dot{x}(t) + f(x(t)) - \sum_{j=1}^k J_j g(x(t), x_j(t)) - \xi(t) \right]. \quad (48)$$

Equations (47) and (48) make up the main analytic result of this work. Interestingly, these equations are formally similar to those determining the eigenvector distribution corresponding to the leading eigenvalue of sparse directed networks [8, 9]. When the degrees K_i and L_i are statistically independent at any node i , the joint degree distribution factorizes, $p_{k, \ell} = p_{\text{in}, k} p_{\text{out}, \ell}$, and the solution of the dynamics reduces to a single self-consistent equation for the path-probability:

$$\mathcal{P}[x] = \sum_{k=0}^{\infty} p_{\text{in}, k} \int \left(\prod_{j=1}^k Dx_j \mathcal{P}[x_j] \right) \int \left(\prod_{j=1}^k dJ_j p_J(J_j) \right) \int D\xi \mathcal{P}_\sigma[\xi] \delta_F \left[\dot{x}(t) + f(x(t)) - \sum_{j=1}^k J_j g(x(t), x_j(t)) - \xi(t) \right]. \quad (49)$$

III. POPULATION DYNAMICS ALGORITHM

Here we explain how to generalize the population dynamics algorithm [1, 3, 10] to efficiently solve the self-consistent Eq. (49) for the path-probability describing dynamical processes on directed random networks with uncorrelated degrees (K_i, L_i) . The algorithm is based on the introduction of a large population of stochastic trajectories that parametrize the path-probability $\mathcal{P}[x]$. These dynamical paths are then consistently updated according to Eq. (49). Informally speaking, the population dynamics algorithm is a Monte-Carlo approach to solve self-consistent distributional equations by iteration, analogous to finding the roots of a transcendental fixed-point equation by direct iteration. In the standard version of the algorithm [1–3], the probability density under study characterizes the statistics of a single random variable, while here one has to generalize the algorithm to deal with the probability density of functions of time. Each stochastic trajectory is constrained to the differential equation imposed by the Dirac functional- δ_F in Eq. (49). The most important aspect of the algorithm in the present case is that a single update refers to an *entire* stochastic trajectory, rather than to a single variable representing a particular instant of time. Apart from this nuance, the core of the algorithm remains conceptually the same as in standard applications.

Below we present a detailed account of the population dynamics algorithm in the absence of Gaussian noise ($\sigma = 0$). For concreteness, we detail all steps of the algorithm on the neural network model of [4], where $f(x) = x$ and $g(x, x') = \tanh(x')$. In this particular setting, Eq. (49) assumes the form

$$\mathcal{P}[x] = \sum_{k=0}^{\infty} p_{\text{in},k} \int \left(\prod_{j=1}^k Dx_j \mathcal{P}[x_j] \right) \int \left(\prod_{j=1}^k dJ_j p_J(J_j) \right) \delta_F \left[\dot{x}(t) + x(t) - h_k [\{J_j, x_j(t)\}] \right], \quad (50)$$

where we defined the time-dependent local field

$$h_k [\{J_j, x_j(t)\}] = \sum_{j=1}^k J_j \tanh(x_j(t)). \quad (51)$$

The extension of the population dynamics algorithm to other models and to nonzero Gaussian noise ($\sigma > 0$) is straightforward.

Algorithm 1 Population dynamics algorithm to solve Eq. (50) and determine the macroscopic observables $m(t)$ and $q(t)$ as a function of time (see Eqs. (9) and (10)). For simplicity, we illustrate the algorithm in conjunction with the Euler method for solving differential equations.

Inputs: indegree distribution $p_{\text{in},k}$, distribution p_J of coupling strengths, population size N_{pop} , total number N_{iter} of single-trajectory updates, total number T of points in a discretized path, and time increment ϵ of the Euler method.

Outputs: macroscopic observables $m(t)$ and $q(t)$ at time t .

Set the indegree distribution $p_{\text{in},k}$ and the distribution $p_J(J)$ of coupling strengths.

Set the matrix $x[t][i]$ ($i = 1, \dots, N_{\text{pop}}$ and $t = 0, \dots, T$) that stores the state variables along the i th dynamical trajectory.

Initialize all matrix elements $x[t][i]$. The entries $\{x[0][i]\}_{i=1, \dots, N_{\text{pop}}}$ fix the initial condition.

repeat

 Select a single element i uniformly at random from the indexes $1, \dots, N_{\text{pop}}$.

 Draw a non-negative random integer k from the distribution $p_{\text{in},k}$.

 Create a set ∂_k with k elements selected uniformly at random from the indexes $1, \dots, N_{\text{pop}}$.

 Create a set with elements J_1, \dots, J_k sampled from the distribution $p_J(J)$.

 Update the local fields $h[1][i], \dots, h[T][i]$ along the trajectory i : $h[t][i] \leftarrow \sum_{j \in \partial_k} J_j \tanh(x[t-1][j])$ \triangleright Eq. (51)

 Update the i th trajectory $x[1][i], \dots, x[T][i]$ (Euler method): $x[t][i] \leftarrow x[t-1][i] + \epsilon(-x[t-1][i] + h[t][i])$

until step number $< N_{\text{iter}}$

return $m(t) \leftarrow \frac{1}{N_{\text{pop}}} \sum_{i=1}^{N_{\text{pop}}} x[t][i]$ and $q(t) \leftarrow \frac{1}{N_{\text{pop}}} \sum_{i=1}^{N_{\text{pop}}} (x[t][i])^2$

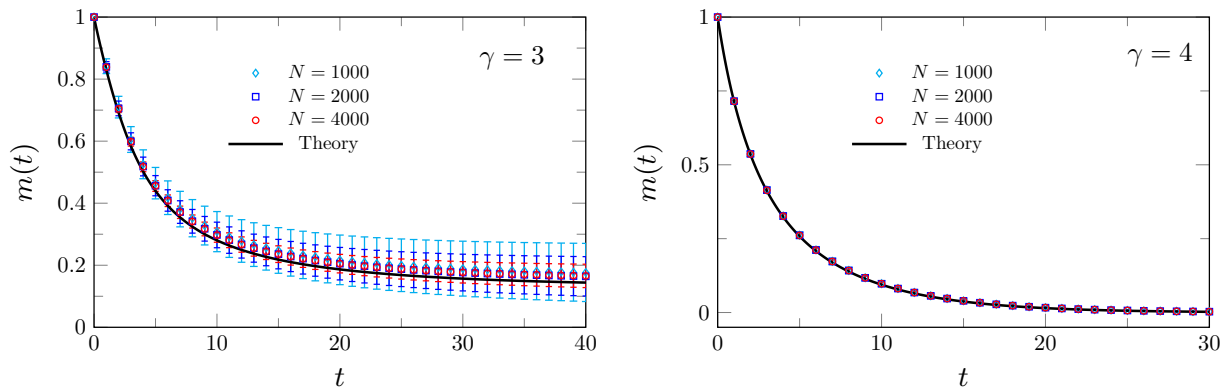


FIG. 1. Dynamics of $m(t)$ for the NN model (see table I in the main text) on directed random networks with a power-law indegree distribution $p_{in,k} = \mathcal{N}k^{-\gamma}$, where \mathcal{N} is the normalization factor and $k \geq 2$. The coupling strengths are drawn from a Gaussian distribution p_J with mean $\mu_J = 1/3$ and standard deviation $\sigma_J = 0.1$. The initial condition for the dynamics is given by $x_i(0) = 1 \forall i$. The solid lines are theoretical results derived from the solutions of Eq. (50) using the population dynamics algorithm with $N_{\text{pop}} = 10^5$. The symbols are obtained from the numerical solutions of Eq. (1) for $h_i(t) = \xi_i(t) = 0$ and an ensemble with 50 independent random networks generated from the configuration model with N nodes. The vertical bars are the standard deviations around the mean values. Left panel: dynamics for the exponent $\gamma = 3$, such that $c \simeq 3.20$ and the model lies in phase II. Right panel: dynamics for the exponent $\gamma = 4$, such that $c \simeq 2.45$ and the model lies in phase I.

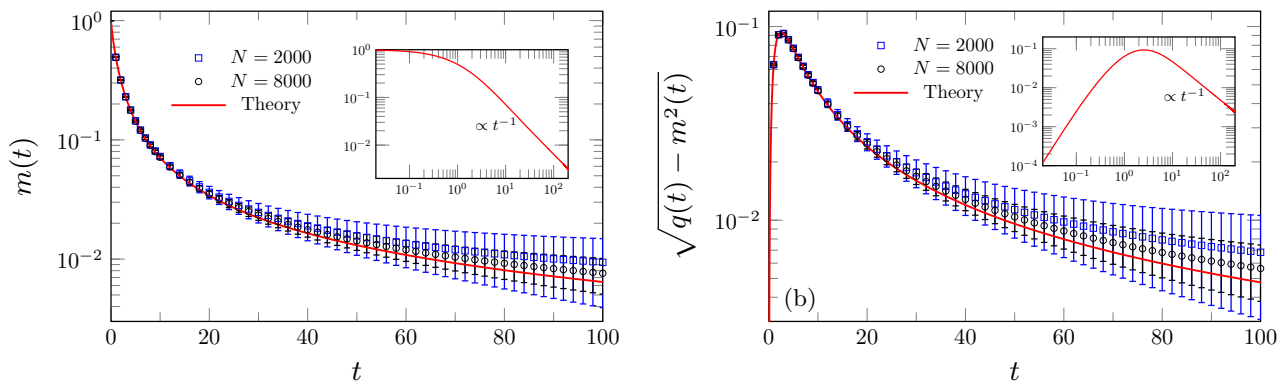


FIG. 2. Dynamics of the mean $m(t)$ and the standard deviation $\sqrt{q(t) - m^2(t)}$ of the local dynamical variables of the SIS model (see table I in the main text) on directed random networks with a Poisson indegree distribution. The coupling strengths are drawn from a uniform distribution p_J with mean $\mu_J = 1/3$ and standard deviation $\sigma_J = 0.1$. The panels show the relaxation dynamics at the critical mean degree $c = \mu_J^{-1}$ that separates the disease-free phase ($m = 0$ for $c < \mu_J^{-1}$) from the endemic phase ($m > 0$ for $c > \mu_J^{-1}$). The initial condition for the dynamics is given by $x_i(0) = 1 \forall i$. The solid red lines are derived from the solutions of Eq. (7) in the main text using the population dynamics algorithm with $N_{\text{pop}} = 10^5$. The symbols are obtained from the numerical solutions of Eq. (1) for $h_i(t) = \xi_i(t) = 0$ and an ensemble with 50 independent random networks generated from the configuration model with N nodes. The insets show the theoretical results in log-log scale.

Let us present results derived from the solutions of Eq. (7) in the main text using the algorithm described above. In the main text, we compare population dynamics with the numerical solutions of the original dynamical equations, Eq. (1), for heterogeneous networks with Poisson and exponential degrees. To further demonstrate the robustness and accuracy of our theoretical approach, we extend this comparison to two different scenarios characterized by strong fluctuations: (i) networks with power-law indegree distributions and (ii) systems prepared at the critical point of a nonequilibrium phase transition. These scenarios are important tests for our theory, as nonequilibrium phase transitions are a ubiquitous feature of complex systems, and power-law degree fluctuations are commonly observed in various real-world networks [11]. Figure (1) illustrates the dynamics of the NN model (see table I in the main text) on networks with a power-law indegree distribution, while Fig. 2 shows results for the relaxation dynamics of the SIS model at the epidemic threshold. In both cases, despite the presence of strong fluctuations in the dynamical variables, the numerical solutions of Eq. (1) consistently converge to the population dynamics results as the system

size N increases. These results further support the exactness of Eq. (7) in the main text for networks with power-law indegrees and for systems at the critical point of a nonequilibrium phase transition. Note, in addition, that the results in Fig. (1) are consistent with the transition between phases I and II (see Fig. 2 in the main text). As shown in Fig. 2, the theoretical results indicate that the mean and the standard deviation of the SIS model decay as $m(t) \propto t^{-1}$ ($t \gg 1$) and $\sqrt{q(t) - m^2(t)} \propto t^{-1}$ ($t \gg 1$) at the epidemic threshold.

In Fig. 3, we present results for the dynamics and the stationary behaviour of $m(t)$ in phases II, III and IV of the NN model (see Fig. 2 in the main text). Figure 3 illustrates the behaviour of the temporal mean

$$M = \frac{1}{T - T_{\text{tr}}} \int_{T_{\text{tr}}}^T dt m(t) \quad (52)$$

and the temporal standard deviation Δ

$$\Delta^2 = \frac{1}{T - T_{\text{tr}}} \int_{T_{\text{tr}}}^T dt [M - m(t)]^2 \quad (53)$$

of the macroscopic variable $m(t)$, where T_{tr} is the transient time after which $m(t)$ stabilizes in an attractor (either fixed-point or chaotic). In the limit $T \rightarrow \infty$, the parameters M and Δ distinguish the different phases of the NN model: $M = 0$ and $\Delta = 0$ in phase I, $M \neq 0$ and $\Delta = 0$ in phase II, $M = 0$ and $\Delta > 0$ in phase III, and $M \neq 0$ and $\Delta > 0$ in phase IV. By numerically solving Eq. (50), we calculate M and Δ for $T \gg 1$ and estimate the transition lines that delimit phase IV. The numerical results for these transitions, shown in Fig. 2 of the main text, are derived by assuming that a nonzero value of $M = \mathcal{O}(10^{-3})$ identifies the transition from the chaotic phase III to phase IV, while a nonzero $\Delta = \mathcal{O}(10^{-4})$ distinguishes phase IV from the fixed-point phase II. For $c = 4$ and $\mu_J = 1/3$, the gap-gapless transition occurs at $\sigma_J = 1/\sqrt{3}$, which is obtained from the equation $c = 1 + \sigma_J^2/\mu_J^2$ (see the dashed line in Fig. 2 of the main text). The value $\sigma_J = 1/\sqrt{3}$ is marked by the vertical dotted line in the middle panel of Fig. 3. Note that this critical value for the gap-gapless transition is consistent with the vanishing of M , which identifies the transition between phases III and IV.

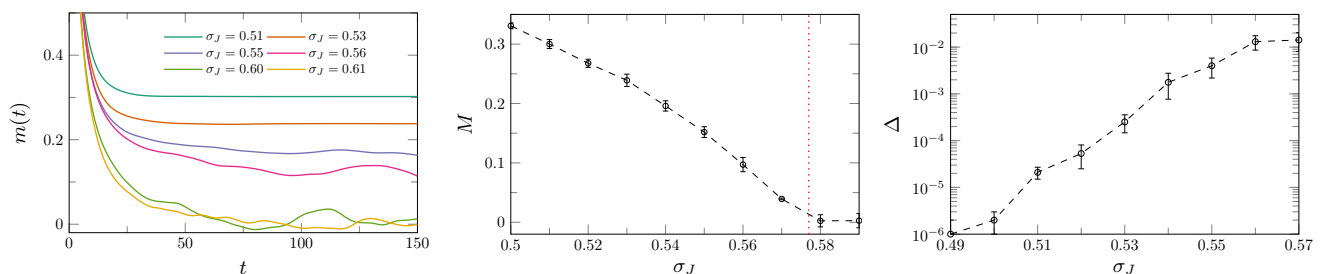


FIG. 3. Behaviour of $m(t)$ for the NN model (see table I in the main text) on directed random networks with a Poisson indegree distribution with mean degree $c = 4$. The random coupling strengths are drawn from a Gaussian distribution p_J with mean $\mu_J = 1/3$ and standard deviation σ_J . The results are derived from the solutions of Eq. (50) using the population dynamics algorithm with $N_{\text{pop}} = 5 \times 10^4$. The panels illustrate the dynamics and the stationary behaviour of $m(t)$ in phases II, III, and IV (see Fig. 2 in the main text). Left panel: dynamics of $m(t)$ for several values of σ_J and initial condition $x_i(0) = 1 \forall i$. Middle panel: temporal average M (see Eq. (52)) of $m(t)$ as a function of σ_J across the transition between phases III and IV. The vertical dotted line marks the gap-gapless transition (see the dashed line in Fig. 2 of the main text). Right panel: temporal standard deviation Δ (see Eq. (53)) of $m(t)$ across the transition between phases II and IV. The results for M and Δ are averaged over five independent realizations of the population dynamics, with the error bars indicating the standard deviation of these realizations.

Finally, we present results that illustrate how the number N_{iter} of single-trajectory updates affects the accuracy of the population dynamics algorithm. Figure 4 shows population dynamics results for the dynamics of $m(t)$ inside phase I of the NN model (see Fig. 2 in the main text) for different values of N_{iter} . We note that, when N_{iter} is not large enough, $m(t)$ evolves to a nontrivial fixed-point, which is not the correct solution predicted by the stability analysis. By increasing the total number N_{iter} of single-trajectory updates, we find that $m(t)$ decays exponentially to $m = 0$, which is the correct solution inside phase I. For the large values of N_{pop} considered in Fig. 4, the results are independent of N_{pop} .

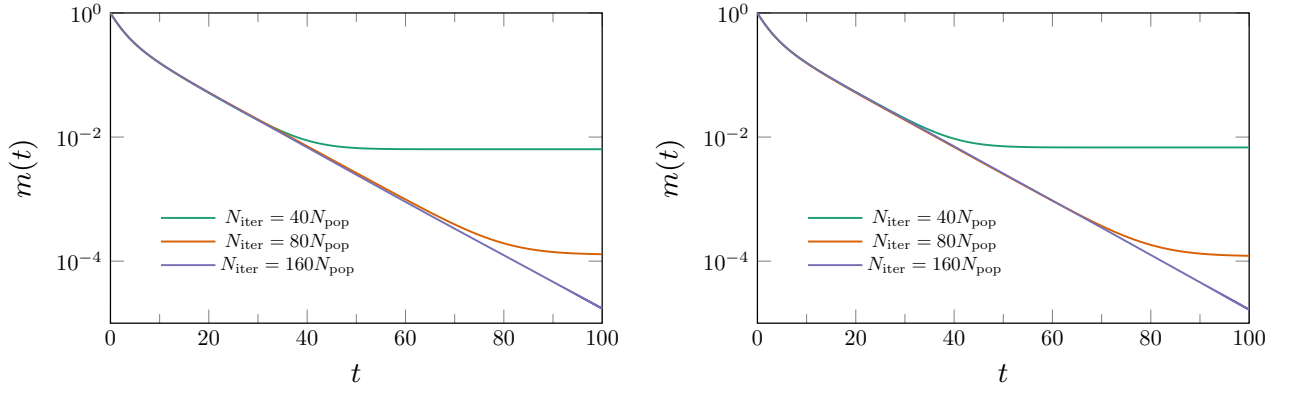


FIG. 4. Dynamics of $m(t)$ for the NN model (see table I in the main text) on directed random networks with a Poisson indegree distribution with mean $c = 2.7$. The coupling strengths are drawn from a Gaussian distribution p_J with mean $\mu_J = 1/3$ and standard deviation $\sigma_J = 0.1$. The initial condition for the dynamics is given by $x_i(0) = 1 \forall i$. These results follow from the solutions of Eq. (50) using the population dynamics algorithm with population size N_{pop} and total number N_{iter} of single-trajectory updates (see the algorithm above). Left panel: $N_{\text{pop}} = 5 \times 10^4$. Right panel: $N_{\text{pop}} = 10^5$.

IV. THE HIGH-CONNECTIVITY LIMIT

An important question is to understand whether the solution of the present class of models converges to the well-known results for fully-connected models as $c \rightarrow \infty$ [4, 12, 13]. Put differently, we aim to probe the universality of fully-connected models in the present context. In a series of recent works [14, 15], it has been shown that spin models on random networks do not converge to their fully-connected counterparts as $c \rightarrow \infty$, but the final solution is determined by the empirical distribution of the degrees rescaled by their mean. In the present context, we also expect that the universality of fully-connected architectures breaks down as $c \rightarrow \infty$, and the path-probability $\mathcal{P}[x]$ retains information about degree fluctuations even in the high-connectivity limit. In this subsection, we explain how to take the limit $c \rightarrow \infty$ of Eq. (49) and obtain the form of $\mathcal{P}[x]$ in the high-connectivity limit. We derive generic analytic results, valid for arbitrary functions $f(x)$ and $g(x, x')$ (see Eq. (1) and table I in the main text), which encapsulates a broad range of important models in the study of complex systems.

By using the functional Fourier transform of the Dirac- δ_F in Eq. (49), we can integrate over the Gaussian noise $\xi(t)$ and obtain the formal expression

$$\mathcal{P}[x] = \int D\hat{x} e^{i \int dt \hat{x}(t)[\dot{\hat{x}}(t) + f(x(t))] - \frac{\sigma^2}{2} \int dt \hat{x}^2(t)} \sum_{k=0}^{\infty} p_{\text{in},k} \exp \left[k \ln \left(\int Dx' \mathcal{P}[x'] \left\langle e^{-iJ \int dt \hat{x}(t)g(x(t), x'(t))} \right\rangle_J \right) \right], \quad (54)$$

where $\langle \dots \rangle_J$ denotes the average over J with respect to its distribution p_J . As we are interested in the high-connectivity limit $c \rightarrow \infty$, it is sensible to rescale the coupling strengths with c in such a way that $\mathcal{P}[x]$ converges to a finite limit. Therefore, we assume that the first two moments of J are given by

$$\int_{-\infty}^{\infty} dJ J p_J(J) = \frac{\mu_J}{c} \quad \text{and} \quad \int_{-\infty}^{\infty} dJ J^2 p_J(J) = \frac{\gamma_J^2}{c}, \quad (55)$$

while higher-order moments of J decay faster than $1/c$. For large c , we can expand the logarithm in Eq. (54) up to $\mathcal{O}(1/c)$, obtaining

$$\begin{aligned} \ln \left(\int Dx' \mathcal{P}[x'] \left\langle e^{-iJ \int dt \hat{x}(t)g(x(t), x'(t))} \right\rangle_J \right) &= -\frac{i\mu_J}{c} \int dt \hat{x}(t) \int Dx' \mathcal{P}[x'] g(x(t), x'(t)) \\ &\quad - \frac{\gamma_J^2}{2c} \int dt dt' \hat{x}(t)\hat{x}(t') \int Dx' \mathcal{P}[x'] g(x(t), x'(t)) g(x(t'), x'(t')). \end{aligned} \quad (56)$$

The above expression depends on functional averages of one-time and two-time quantities with respect to the path-probability $\mathcal{P}[x']$. By defining the conditional macroscopic parameters

$$M(t|x(t)) = \int Dx' \mathcal{P}[x'] g(x(t), x'(t)) \quad \text{and} \quad C(t, t'|x(t), x(t')) = \int Dx' \mathcal{P}[x'] g(x(t), x'(t)) g(x(t'), x'(t')), \quad (57)$$

the logarithmic contribution can be written in the compact form

$$\ln \left(\int D x' \mathcal{P}[x'] \left\langle e^{-iJ \int dt \hat{x}(t) g(x(t), x'(t))} \right\rangle_J \right) = -\frac{i\mu_J}{c} \int dt \hat{x}(t) M(t|x(t)) - \frac{\gamma_J^2}{2c} \int dt dt' \hat{x}(t) \hat{x}(t') C(t, t'|x(t), x(t')). \quad (58)$$

Inserting the above expression back into Eq. (54) and introducing the distribution of rescaled indegrees [14, 15],

$$\nu_{\text{in}}(\kappa) = \lim_{c \rightarrow \infty} \sum_{k=0}^{\infty} p_{\text{in},k} \delta \left(\kappa - \frac{k}{c} \right), \quad (59)$$

we get

$$\begin{aligned} \mathcal{P}[x] &= \int_0^{\infty} d\kappa \nu_{\text{in}}(\kappa) \int D\hat{x} \exp \left(i \int dt \hat{x}(t) [\dot{x}(t) + f(x(t)) - \mu_J \kappa M(t|x(t))] \right) \\ &\quad \times \exp \left(-\frac{1}{2} \int dt dt' \hat{x}(t) \hat{x}(t') [\sigma^2 \delta(t-t') + \gamma_J^2 \kappa C(t, t'|x(t), x(t'))] \right). \end{aligned} \quad (60)$$

Finally, we can define the conditional covariance matrix

$$\Delta_{\kappa}(t, t'|x(t), x(t')) = \sigma^2 \delta(t-t') + \gamma_J^2 \kappa C(t, t'|x(t), x(t')) \quad (61)$$

and rewrite Eq. (60) as follows

$$\mathcal{P}[x] = \int_0^{\infty} d\kappa \nu_{\text{in}}(\kappa) \int D\omega \mathcal{P}[\omega|\kappa] \delta_F \left[\dot{x}(t) + f(x(t)) - \mu_J \kappa M(t|x(t)) - \omega(t) \right], \quad (62)$$

where $\omega(t)$ is a temporally correlated noise with the functional distribution

$$\mathcal{P}[\omega|\kappa] = \frac{1}{\mathcal{N}_{\omega}} \exp \left(-\frac{1}{2} \int dt dt' \omega(t) \omega(t') \Delta_{\kappa}^{-1}(t, t'|x(t), x(t')) \right), \quad (63)$$

conditioned to a fixed rescaled degree κ . The factor \mathcal{N}_{ω} ensures that $\int D\omega \mathcal{P}[\omega|\kappa] = 1$.

Equation (62) gives the analytic form of the path-probability density in the limit $c \rightarrow \infty$. Clearly, $\mathcal{P}[x]$ is determined by the distribution $\nu_{\text{in}}(\kappa)$ of rescaled indegrees, which means that the effective dynamics retains information about the network degree fluctuations even in the limit $c \rightarrow \infty$. Put differently, Eq. (62) demonstrates that the effective dynamics of fully-connected networks is not universal, in the sense that models on sparse networks do not generally flow to their fully-connected counterparts as the mean degree c diverges. This (perhaps surprising) nonuniversal character is not exclusive to the continuous-time dynamics of complex systems, but it has been previously identified in the context of Ising spin models [14, 15] and random matrix theory [16, 17].

For homogeneous networks, in which the indegree distribution $p_{\text{in},k}$ is such that $\nu_{\text{in}}(\kappa) = \delta(\kappa - 1)$, we expect to recover previous analytic results for the effective dynamics of models on fully-connected networks. Typical examples of homogeneous networks are regular networks ($p_{\text{in},k} = \delta_{k,c}$) and networks with Poisson indegrees ($p_{\text{in},k} = c^k e^{-c}/k!$). In both cases, it is straightforward to check from Eq. (59) that $\nu_{\text{in}}(\kappa) = \delta(\kappa - 1)$. Let us explicitly recover previous analytic results in the case of homogeneous networks. Here we focus on two particular examples: the Lotka-Volterra (LV) model and the neural network (NN) model of [4]. For the NN model, we have $f(x) = x$ and $g(x, x') = \tanh(x')$, and Eq. (62) assumes the form

$$\mathcal{P}_{\text{NN}}[x] = \int_0^{\infty} d\kappa \nu_{\text{in}}(\kappa) \int D\omega \mathcal{P}[\omega|\kappa] \delta_F \left[\dot{x}(t) + x(t) - \mu_J \kappa M(t) - \omega(t) \right], \quad (64)$$

where the covariance of $\omega(t)$ reads

$$\Delta_{\kappa}(t, t') = \sigma^2 \delta(t-t') + \gamma_J^2 \kappa C(t, t'), \quad (65)$$

with

$$M(t) = \int Dx \mathcal{P}[x] \tanh(x(t)) \quad \text{and} \quad C(t, t') = \int Dx \mathcal{P}[x] \tanh(x(t)) \tanh(x(t')). \quad (66)$$

Equations (64-66) enable to study the role of indegree heterogeneities in the high-connectivity limit of the NN model. As expected, when $\nu_{\text{in}}(\kappa) = \delta(\kappa - 1)$, Eqs. (64-66) reduce to the equations describing the effective dynamics of fully-connected models with Gaussian interactions [4, 5, 18]. For the LV model, we have that $f(x) = x(x - 1)$ and $g(x, x') = xx'$, and the path-probability becomes

$$\mathcal{P}_{\text{LV}}[x] = \int_0^\infty d\kappa \nu_{\text{in}}(\kappa) \int D\omega \mathcal{P}[\omega|\kappa] \delta_F \left[\dot{x}(t) + x(t)(x(t) - 1) - \mu_J \kappa x(t)M(t) - \omega(t) \right], \quad (67)$$

where the covariance of $\omega(t)$ reads

$$\Delta_\kappa(t, t'|x(t), x(t')) = \sigma^2 \delta(t - t') + \gamma_J^2 \kappa x(t)x(t')C(t, t'), \quad (68)$$

with

$$M(t) = \int Dx \mathcal{P}[x] x(t) \quad \text{and} \quad C(t, t') = \int Dx \mathcal{P}[x] x(t)x(t'). \quad (69)$$

When $\nu_{\text{in}}(\kappa) = \delta(\kappa - 1)$ and $\sigma = 0$, Eqs. (67-69) yield the effective dynamics of the corresponding fully-connected Lotka-Volterra model with Gaussian interactions [19]. The results obtained here for the Lotka-Volterra model in the limit $c \rightarrow \infty$ are closely related to recent works [20, 21].

Finally, we discuss the correspondence between the phase diagram of the fully-connected version of the NN model (see Figure 1 in [22]) and Fig. 2 in the main text as $c \rightarrow \infty$. The linear stability of the trivial solution $\mathbf{x} = 0$ is governed by the real part of leading eigenvalue λ_1 of the adjacency matrix \mathbf{A} . If $\text{Re}\lambda_1 < 1$, the trivial solution is stable. By rescaling the moments of the coupling strengths in the sparse directed network as $\mu_J = J_0/c$ and $\sigma_J^2 = g^2/c$, the spectrum of \mathbf{A} converges, in the limit $c \rightarrow \infty$, to a uniform disc of radius $|\lambda| = g$ in the complex plane [3, 8, 9]. Additionally, when $J_0 > g$, the dense matrix \mathbf{A} has an outlier eigenvalue at $\lambda = J_0$. Thus, combining these results for the leading eigenvalue λ_1 with the condition $\text{Re}\lambda_1 < 1$, we find that, in the limit $c \rightarrow \infty$, $\mathbf{x} = 0$ is stable when both $J_0 < 1$ and $g < 1$, while the straight line $J_0 = g$ represents the gap-gapless transition. Hence, the transition lines delimiting the stability of $\mathbf{x} = 0$ agree with the results in [22], while the transition to the homogeneous chaotic phase III in the phase diagram (J_0, g) of [22] slightly deviates from the straight line $J_0 = g$ marking the gap-gapless transition in the network spectrum.

-
- [1] M Mézard and G Parisi, “The bethe lattice spin glass revisited,” *Eur. Phys. J. B* **20**, 217–233 (2001).
 - [2] M Mézard and G Parisi, “The cavity method at zero temperature,” *J. Stat. Phys.* **111**, 1–34 (2003).
 - [3] Fernando Lucas Metz, Izaak Neri, and Tim Rogers, “Spectral theory of sparse non-hermitian random matrices,” *Journal of Physics A: Mathematical and Theoretical* **52**, 434003 (2019).
 - [4] H. Sompolinsky, A. Crisanti, and H. J. Sommers, “Chaos in random neural networks,” *Phys. Rev. Lett.* **61**, 259–262 (1988).
 - [5] A. Crisanti and H. Sompolinsky, “Path integral approach to random neural networks,” *Phys. Rev. E* **98**, 062120 (2018).
 - [6] J P L Hatchett, B Wemmenhove, I Pérez Castillo, T Nikolettopoulos, N S Skantzios, and A C C Coolen, “Parallel dynamics of disordered ising spin systems on finitely connected random graphs,” *Journal of Physics A: Mathematical and General* **37**, 6201 (2004).
 - [7] Kazushi Mimura and A C C Coolen, “Parallel dynamics of disordered ising spin systems on finitely connected directed random graphs with arbitrary degree distributions,” *Journal of Physics A: Mathematical and Theoretical* **42**, 415001 (2009).
 - [8] Izaak Neri and Fernando Lucas Metz, “Linear stability analysis of large dynamical systems on random directed graphs,” *Phys. Rev. Res.* **2**, 033313 (2020).
 - [9] Fernando Lucas Metz and Izaak Neri, “Localization and universality of eigenvectors in directed random graphs,” *Phys. Rev. Lett.* **126**, 040604 (2021).
 - [10] Reimer Kühn, “Spectra of sparse random matrices,” *Journal of Physics A: Mathematical and Theoretical* **41**, 295002 (2008).
 - [11] M. Newman, *Networks: An Introduction* (OUP Oxford, 2010).
 - [12] Guy Bunin, “Ecological communities with lotka-volterra dynamics,” *Phys. Rev. E* **95**, 042414 (2017).
 - [13] Carles Martorell, Rubén Calvo, Alessia Annibale, and Miguel A. Muñoz, “Dynamically selected steady states and criticality in non-reciprocal networks,” *Chaos, Solitons and Fractals* **182**, 114809 (2024).
 - [14] Fernando L Metz and Thomas Peron, “Mean-field theory of vector spin models on networks with arbitrary degree distributions,” *Journal of Physics: Complexity* **3**, 015008 (2022).
 - [15] Leonardo S. Ferreira and Fernando L. Metz, “Nonequilibrium dynamics of the ising model on heterogeneous networks with an arbitrary distribution of threshold noise,” *Phys. Rev. E* **107**, 034127 (2023).

- [16] Fernando L. Metz and Jeferson D. Silva, “Spectral density of dense random networks and the breakdown of the wigner semicircle law,” *Phys. Rev. Res.* **2**, 043116 (2020).
- [17] Jeferson D Silva and Fernando L Metz, “Analytic solution of the resolvent equations for heterogeneous random graphs: spectral and localization properties,” *Journal of Physics: Complexity* **3**, 045012 (2022).
- [18] Jannis Schuecker, Sven Goedeke, and Moritz Helias, “Optimal sequence memory in driven random networks,” *Phys. Rev. X* **8**, 041029 (2018).
- [19] Tobias Galla, “Dynamically evolved community size and stability of random lotka-volterra ecosystems(a),” *Europhysics Letters* **123**, 48004 (2018).
- [20] Jong Il Park, Deok-Sun Lee, Sang Hoon Lee, and Hye Jin Park, “Incorporating heterogeneous interactions for ecological biodiversity,” *Phys. Rev. Lett.* **133**, 198402 (2024).
- [21] Fabián Aguirre-López, “Heterogeneous mean-field analysis of the generalized lotka-volterra model on a network,” *Journal of Physics A: Mathematical and Theoretical* **57**, 345002 (2024).
- [22] Francesca Mastrogioseppe and Srdjan Ostojic, “Linking connectivity, dynamics, and computations in low-rank recurrent neural networks,” *Neuron* **99**, 609–623.e29 (2018).